Geochimica et Cosmochimica Acta 364 (2024) 195–210

Contents lists available at ScienceDirect

Geochimica et Cosmochimica Acta

journal homepage: www.elsevier.com/locate/gca

Questioning the role of methane in the wake of a snowball Earth: Insights from isotopically anomalous cap dolostone cements with a complex diagenetic history

Huan Cui [a,b,*], Kouki Kitajima [b], Ian J. Orland [b,c], Jean-Marc Baele [d], Adam Denny [b,e], Michael J. Spicuzza [b], John H. Fournelle [b], Steven Goderis [f], Niels J. de Winter [f,g], John W. Valley [b]

[a] Department of Geosciences, Mississippi State University, Mississippi State, MS 39762, USA
[b] Department of Geoscience, University of Wisconsin-Madison, Madison, WI, 53706, USA
[c] Wisconsin Geological and Natural History Survey, University of Wisconsin-Madison, Madison, WI, 53705, USA
[d] Department of Geology and Applied Geology, Faculty of Engineering, University of Mons, 7000 Mons, Belgium
[e] Pacific Northwest National Laboratory, Richland, WA 99354, USA
[f] Archaeology, Environmental Changes and Geo-Chemistry Group, Vrije Universiteit Brussel, 1050 Brussels, Belgium
[g] Department of Earth Sciences, Faculty of Science, Vrije Universiteit Amsterdam, 1081 HV Amsterdam, the Netherlands

A R T I C L E I N F O

Associate editor: Eva Stüeken

Keywords:
Authigenic carbonate
Methane seeps
Methane clathrate
Cap dolostones
Secondary ion mass spectrometry

A B S T R A C T

Methane has been widely regarded as an important source of greenhouse gas that modulated Earth's paleoclimate. Notably, it has been proposed that a massive release of methane via clathrate destabilization may have played a critical role during and/or in the immediate aftermath of the Marinoan deglaciation. One key piece of supporting evidence for this hypothesis comes from the isotopically anomalous ($\delta^{13}C_{carb}$ < −30 ‰) methane-derived authigenic calcite (MDAC) cements within post-Marinoan cap dolostones in South China. However, the origin of these MDAC cements remains hotly contested, including a clumped isotope study that reinterpreted them as resulting from late hydrothermal fluids. To further evaluate these critical yet controversial cements, a detailed investigation by secondary ion mass spectrometry (SIMS) was conducted. Here we report the largest range of $\delta^{13}C_{carb}$ values (−53.1 ‰ to +6.3 ‰) yet measured in Precambrian carbonates. Our study shows that the MDAC cements are post-depositional, void-filling, and rich in Mn. Importantly, integrated petrographic and SIMS results consistently show that MDAC cements post-date disrupted dolomite laminae that bear surprisingly positive $\delta^{13}C_{carb}$ values up to +6.3 ‰. This is the first report that authigenic carbonates with positive $\delta^{13}C_{carb}$ signals are found within post-Marinoan cap dolostone. Although the precise age of these authigenic carbonates remains ambiguous, integrated chemostratigraphic and SEM-SIMS results suggest that the dolomite laminae formed after the deposition of the uppermost cap dolostone interval, when the seawater $\delta^{13}C$ had already evolved to positive values; and the MDAC formed even later. The dolomite laminae and MDAC cements, therefore, represent distinct post-depositional, exogenous, diagenetic carbon signals that are irrelevant to the deglaciation. Our new results challenge the hypothesis that methane played a central role at the end of or in the immediate aftermath of the Marinoan glaciation. Rather, the infiltration of methane-bearing fluids within cap dolostones could have occurred much later.

1. Introduction

Methane seeps (also known as cold seeps) are common in modern marine environments and have also been widely discovered in the ancient geological record (Peckmann and Thiel, 2004; Campbell, 2006). However, unequivocal evidence for methane seeps in the Precambrian strata is remarkably rare (Bristow and Grotzinger, 2013). To our knowledge, purported Precambrian methane seeps have been reported from only three intervals, including the terminal Cryogenian glacial diamictite interval in South Australia (Kennedy et al., 2008) and the

* Corresponding author at: Department of Geosciences, Mississippi State University, Mississippi State, MS 39762, USA.
E-mail address: Huan.Cui@geosci.msstate.edu (H. Cui).

https://doi.org/10.1016/j.gca.2023.11.002
Received 19 August 2023; Accepted 4 November 2023
Available online 7 November 2023

early Ediacaran cap dolostone intervals in the Nanhua Basin of South China (Jiang et al., 2003; Jiang et al., 2006b; Wang et al., 2008; Peng et al., 2022) and the Taoudeni Basin of Mali (Shields et al., 2007; Álvaro et al., 2023). Notably, all these three intervals are closely associated with the Cryogenian-Ediacaran boundary (ca. 635 Ma), where cap dolostones with negative $\delta^{13}C_{carb}$ values (mostly 0 to ~–5‰, VPDB) were deposited right above glacial diamictite at a global scale in the wake of the Marinoan glaciation (also known as the snowball Earth) (Hoffman et al., 1998; Hoffman, 2011). Given the close stratigraphic association with the Marinoan snowball Earth event, these interpreted methane seeps have been proposed to be the key evidence for the involvement of methane clathrate destabilization during and/or in the immediate aftermath of the snowball Earth deglaciation (Jiang et al., 2003; Kennedy et al., 2008; Peng et al., 2022).

Geochemical analyses based on micro-drilled powders reveal that the above-mentioned Precambrian methane seeps show anomalous $\delta^{13}C_{carb}$ or $\delta^{18}O_{carb}$ values. Authigenic calcite cements within cap dolostones in South China and Mali show extremely negative $\delta^{13}C_{carb}$ values down to –48 ‰ (Jiang et al., 2003; Jiang et al., 2006a; Wang et al., 2008; Peng et al., 2022) and –43 ‰ (Álvaro et al., 2023), respectively. In contrast, the inferred methane seeps in Australia show only mildly negative $\delta^{13}C_{carb}$ values (down to –8‰) but anomalously positive $\delta^{18}O_{carb}$ values (up to +12 ‰, VPDB) (Kennedy et al., 2008). The identification of Precambrian methane seeps within these intervals heavily relies on the interpretation of these geochemical signals.

However, the origin of the methane-derived authigenic calcite (MDAC) in South China has been highly contested. On the one hand, these isotopically anomalous cements have been proposed to have formed during destabilization and oxidation of methane hydrates in the aftermath of Marinoan glaciation (Jiang et al., 2003; Jiang et al., 2006a; Jiang et al., 2006b; Wang et al., 2008). On the other hand, the same MDAC cements have also been reinterpreted as post-depositional, possibly very late diagenetic carbonates that are irrelevant to the deglaciation (Bristow et al., 2011; Lin et al., 2011; Zhou et al., 2017). Notably, a clumped isotope study suggests that the MDAC in South China likely formed during hydrothermal activities at temperatures >450 °C in early Cambrian — almost 100 million years after the Marinoan glaciation (Bristow et al., 2011). More recently, it has been proposed that these MDAC cements, albeit post-depositional, formed within ~50 ky since the onset of the deglaciation and thus still bear a close temporal link to the post-Marinoan marine environment (Peng et al., 2022).

Though intensively studied, precise age constraints for the basal Doushantuo authigenic carbonates remain limited. Notably, three U-Pb ages have been published based on in situ dating of carbonates by laser ablation. A U-Pb age of 632 ± 17 Ma was measured from isopachous dolomite cements and has been linked to cap dolostone karstification prior to MDAC precipitation (Gan et al., 2021). A U-Pb age of 636.5 ± 7.4 Ma was measured from calcite cements in the "grape-structured dolostone" that were assumed to bear methane signals but have not been directly tested for $\delta^{13}C_{carb}$ (Lan et al., 2022). More recently, a U-Pb age of 593.7 ± 8.7 Ma was obtained directly from calcite cements with $\delta^{13}C_{carb}$ of –26.8 ‰ (Shi et al., 2023). The above three ages generally have a rather large error and, therefore, warrant further investigation.

Although these controversial authigenic carbonates have been intensively studied, published studies are mostly based on micro-drilled powders (~800-µm spot size) or laser ablation (~100-µm spot size), which commonly yield ambiguous signals due to the mixture of petrographically complex and isotopically disparate phases. In this study, we aim to further characterize the geochemical signature of each individual phase via integrated secondary ion mass spectrometry (SIMS, 7-µm-diameter spot size), cathodoluminescence (CL), micro-X-Ray Fluorescence (µXRF), scanning electron microscope (SEM), energy-dispersive spectrometry (EDS), and electron probe microanalysis (EPMA). Based on the new results with micron-scale spatial resolution, we reconstruct the paragenetic sequence of these authigenic carbonates and evaluate their purported causal links to the snowball Earth deglaciation.

2. Geological Background

The early Ediacaran (post-Marinoan) cap dolostone is a dolomicrite-dominated interval right above the Marinoan glacial deposits (Hoffman, 2011). Field observations show a close coupling between cap dolostone and Marinoan glacial diamictite across the Cryogenian-Ediacaran boundary at a global scale (Hoffman et al., 2011), including the basal Doushantuo Formation where the Doushantuo cap dolostone overlies the Nantuo diamictite across the Nanhua basin in South China (Wang et al., 1981; Jiang et al., 2006a; Jiang et al., 2011). Geochronological studies in the past decades have constrained the Cryogenian-Ediacaran boundary to be ca. 635 Ma (Hoffmann et al., 2004; Condon et al., 2005; Prave et al., 2016; Yang et al., 2021). The duration of cap dolostone deposition remains contested (Hoffman et al., 2017). Notably, sedimentological and numerical modelling studies suggest a duration of around 10^3–10^4 yr based on the timescale of ice-sheet meltdown and whole-ocean warming (Hoffman et al., 2017; Yang et al., 2017), which is supported by an independent geochemical model (Crockford et al., 2016).

Detailed mechanisms of cap dolostone deposition remain debated. The methane hydrate hypothesis predicts a scenario of carbonate deposition coupled with gas hydrate oxidation during deglaciation (Kennedy et al., 2001), whereas the hard snowball Earth hypothesis indicates a depositional process driven by a large reservoir of dissolved alkalinity built-up during the Snowball Earth event as well as via enhanced chemical weathering during deglaciation (Hoffman et al., 1998; Hoffman and Schrag, 2002). In addition, an updated conceptual model – characterized by a meltwater plume that physically separates the surface and deep ocean reservoirs during deglaciation – has also been proposed (Shields, 2005; Yang et al., 2017) and increasingly been invoked by more recent geochemical studies (Liu et al., 2018; Ahm et al., 2019; Wei et al., 2019). Notably, it has been proposed that a delay in cap dolostone precipitation may occur after deglaciation; and that cap dolostone deposition did not start until chemical weathering consumed substantial amounts of atmospheric CO_2 and accumulated high levels of oceanic alkalinity (Huang et al., 2016). In addition, surface ocean warming (Fabre et al., 2013) and enhanced alkalinity contributed by chemical weathering (Fabre and Berger, 2012) have also been proposed to be strong controlling factors for cap carbonate deposition. In terms of mineralogy, an integrated Ca and Mg isotope study suggests that the early Ediacaran cap dolostones formed via early diagenetic dolomitization of aragonite (Ahm et al., 2019).

The basal Doushantuo cap dolostone in South China has been intensively studied over the past two decades. This interval shows typical sheet cracks, tepee-like structures, and barite crystal fans (Jiang et al., 2006a; Zhou et al., 2010; Xiao et al., 2012; Cui et al., 2019), which is highly consistent with correlative strata at a global scale (Hoffman and Macdonald, 2010; Hoffman et al., 2011; Crockford et al., 2018). Barite crystal fans with anomalous ^{17}O depletion have been reported in South China and are interpreted as the evidence for ultra-high pCO_2 (350 times present atmospheric level) in the aftermath of the Marinoan glaciation (Bao et al., 2000; Peng et al., 2011; Killingsworth et al., 2013). Based on a basin-scale stratigraphic correlation of published $\delta^{13}C_{carb}$ profiles and U-Pb ages, this ^{17}O-depletion event has been proposed to last for less than 1 My (Cao and Bao, 2013; Killingsworth et al., 2013).

The temporal relationship between the ^{17}O-depletion event and the purported methane seep activity is a matter of ongoing investigation. Based on detailed petrographic observations, it was proposed that the ^{17}O-depletion event pre-dates the methane seep activity in South China (Zhou et al., 2010). More recently, largely based on regional stratigraphic correlations, it has also been proposed that methane seep activity coincided with the earliest Ediacaran ^{17}O-depletion episode, and occurred within ~50 ky since the onset of the deglaciation (Peng et al., 2022).

Detailed geological background of the Doushantuo cap dolostones has been published in previous studies (Jiang et al., 2006a; Jiang et al., 2011). The cap dolostone interval in the basal Doushantuo Formation of South China overlies the Marinoan Nantuo diamictite and has been subdivided into three units (i.e., C1 to C3 in ascending stratigraphic order, Fig. 1B) based on their distinct sedimentological features in the Yangtze Gorges region (Jiang et al., 2003; Jiang et al., 2006a). Unit C1 represents the interval right above the Nantuo glacial diamictite and is characterized by strongly disrupted dolomite with abundant fractures, bedding-parallel sheet cracks, localized breccias, and stromatactis-like cavities. The cap dolostone C2 interval consists of laminated dolostone with microbial fabrics, tepee-like structures, and sheet-cracks. The cap dolostone C3 interval typically shows laminated limestone. Previous studies show that the MDAC typically occurs as multiple generations of cements in voids, cavities, and crusts on breccias or as thin lenses that are parallel to the bedding of the cap dolostones (Jiang et al., 2006a; Wang et al., 2008; Zhou et al., 2010; Zhou et al., 2016; Peng et al., 2022).

The stratigraphic division the Doushantuo cap dolostones has been slightly changed over time. Due to the similar features between C3 and the overlying Member II carbonates, many more recent studies have abandoned the C3 interval and only divided the cap dolostones to two

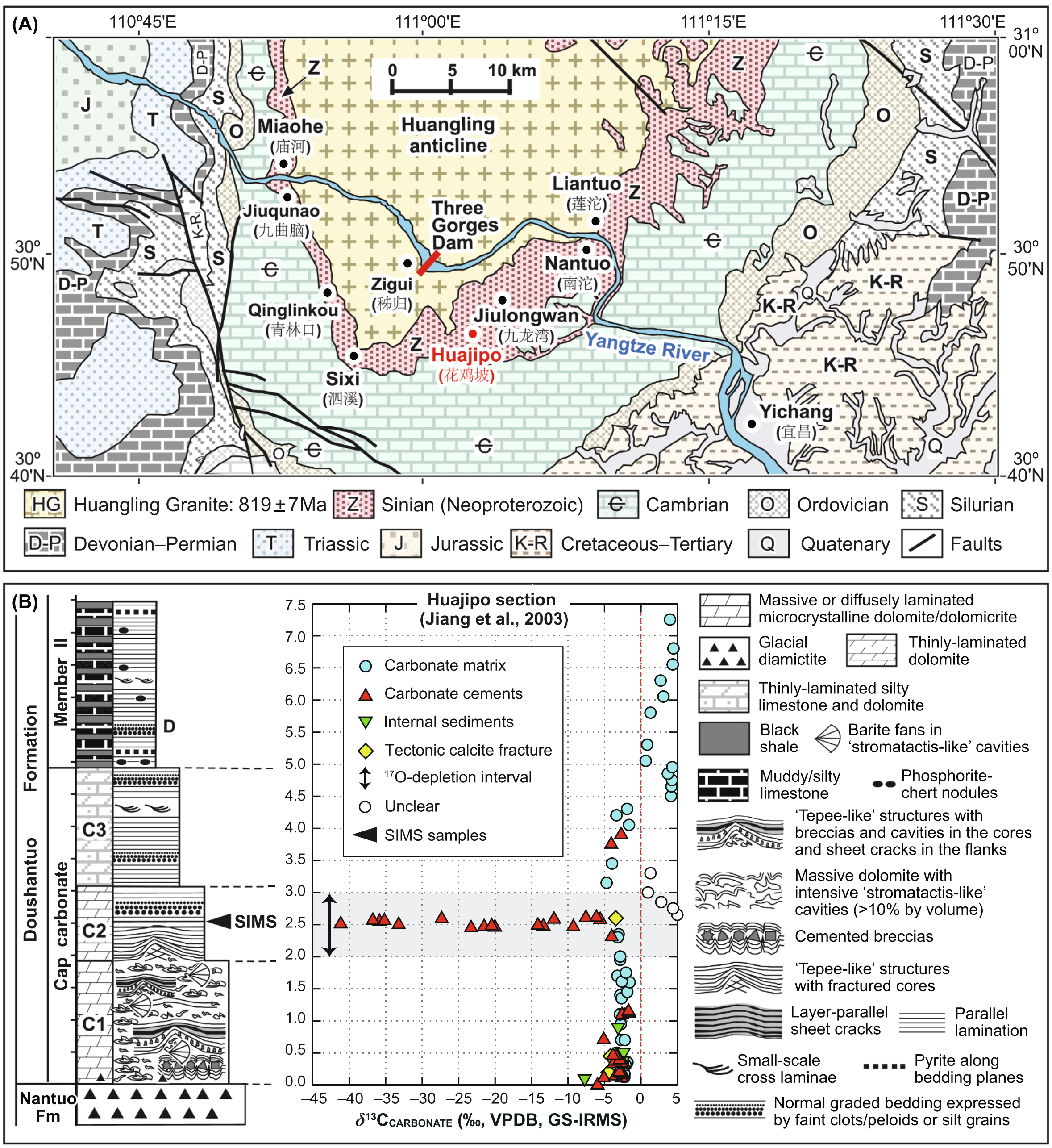

Fig. 1. Geological context of the SIMS samples investigated in this study. (A) Geological map of the Yangtze Gorge area, South China. SIMS samples in this study were collected from the cap dolostone C2 interval, Doushantuo Formation, Huajipo (shown as red dot), South China. (B) Lithological column (in meters) and carbonate carbon isotope ($\delta^{13}C_{carb}$) data analyzed by traditional gas-source isotope ratio mass spectrometer. The cap dolostone interval in South China is commonly subdivided to three units (i.e., C1, C2, and C3) based on distinct sedimentological features (Jiang et al., 2003; Jiang et al., 2006a). Note that the C2 interval overlaps the ^{17}O-depletion interval. Data source: geological map (Zhang et al., 2005); lithological column and carbon isotope data (Jiang et al., 2003; Jiang et al., 2006a); ^{17}O-depletion interval (Peng et al., 2022). Abbreviations: GS-IRMS, gas source-isotope ratio mass spectrometry; SIMS, secondary ion mass spectrometry; VPDB, Vienna Pee Dee Belemnite.

intervals (Lang et al., 2016; Zhou et al., 2016; Wang et al., 2017; Ning et al., 2021), which approximately correspond to C1 and C2 in earlier papers. It is also worth mentioning that the outcrop that was originally reported to preserve extremely low $\delta^{13}C_{carb}$ signals (i.e., Section 3 in Jiang et al., 2003) has later been revised to be "Section 4 (Huajipo)" by Jiang et al., (2006a). Therefore, we adopted the section name "Huajipo" in this study (Fig. 1).

3. Samples and methods

The samples in this study come from the cap dolostone C2 interval, basal Doushantuo Formation at the Huajipo section, South China (Fig. 1). This is the same stratigraphic interval at the same section that was originally analyzed for $\delta^{13}C_{carb}$ (based on micro-drilled powder) as the key evidence for the methane hydrate hypothesis (Jiang et al., 2003; Jiang et al., 2006a) and also has been studied for clumped isotope thermometry (based on micro-drilled powder) providing the key evidence for the hydrothermal fluid hypothesis (Bristow et al., 2011).

More specifically, the samples are preserved as multiple stages of distinct authigenic carbonate infillings within a carbonate cavity in the cap dolostone interval at 2.5 to 2.6 m above the Nantuo and Doushantuo boundary. These coarse-grained authigenic precipitates are in strong contrast with the cap dolostone host rock, which is typically characterized by homogeneous dolomicrite or fine-grained peloidal dolopackstone (see petrographic images Fig. 7A and B in Jiang et al., 2006a).

Previously published $\delta^{13}C_{carb}$ data measured from the same sample were based on micro-drilled powders (see Fig. 13 in Jiang et al., 2006a). In this study, seven epoxy mounts (25.4 mm in diameter) were newly analyzed by SEM and SIMS (Fig. 3, Figs. A1–A9). Detailed descriptions of the analytical methods can be found in our earlier papers (Xiao et al., 2020; Cui et al., 2021; Cui et al., 2022) and are briefly summarized below.

3.1. Micro-X-ray Fluorescence analysis

Seven polished and carbon coated SIMS plugs were analyzed using micro-X-Ray Fluorescence (μXRF) scanning. High-resolution elemental abundance maps of the polished sample surfaces (Fig. 3, Figs. A6–A12) were produced using a Bruker M4 Tornado μXRF scanner (Bruker nano GmbH, Berlin, Germany) at the AMGC research unit of the Vrije Universiteit Brussel, Brussels, Belgium. The measurement was carried out under vacuum (20 mbar) conditions to prevent interference of air. A detailed schematic overview of the M4 Tornado's XRF setup is given in de Winter and Claeys (2017).

The M4 Tornado was equipped with a 30 W metal-ceramic Rh X-ray source and operated under maximum energy settings (50 kV, 600 μA). No source filter was used for incoming X-rays. The X-ray beam was focused on a circular spot on the surface of the sample measuring 25 μm in diameter (calibrated for Mo-Kα radiation) using polycapillary optics. Two XFlash silicon drift detectors were positioned to capture outgoing fluorescence radiation whose trajectory typically showed a total angle of 90° at the surface with respect to the incoming X-ray beam. Carbon coating on the sample could not influence the XRF measurements, as the energy of fluorescence photons of carbon (0.282 keV) typically falls outside the detectible range of the XFlash detectors (~1 keV–25 keV).

The μXRF mapping was performed along a 2D grid with 25 μm spacing, a spot size of 25 μm and an integration time of 1 ms per pixel. This mapping approach resulted in qualitative element concentration distributions on the elemental maps. The full surface of the SIMS plugs was mapped by continuously rastering the 25 μm X-ray beam across the surface in horizontal scanning lines and collecting X-ray counts in discrete time intervals that are treated as map pixels. The XYZ stage enables 1-μm precision sample positioning during measurement. This method allows data collection with a high spatial resolution, albeit with low integration times per pixel. The typical 1 ms integration time per pixel enables semi-quantitative mapping of relative element distributions throughout the samples. However, the short measurement time does not allow the Time of Stable Reproducibility and Accuracy to be reached [see discussion in de Winter et al. (2017)], and therefore does not allow confident pixel-by-pixel quantification of the maps. Prominent X-ray Fluorescence Kα peaks of Ca, Mn and Fe were identified and integrated for every pixel spectrum to produce maps of X-ray Fluorescence intensity (in XRF counts per element) across the sample surface.

3.2. Cathodoluminescence imaging

Cathodoluminescence (CL) images in this study were generated by a cold-cathode CITL CL system (Cambridge Image Technology – model Mk5, UK) in the Department of Geology, University of Mons, Belgium. The cold-cathode CL instrument was operated in the conditions of 15 kV acceleration voltage, 500 μA beam current, and a current density of about 8 μA/mm^2. CL images were captured with a Peltier-cooled digital color camera (Lumenera model Infinity 3, Canada) set from 0.1 s to a few seconds exposure time depending on the CL intensity and microscope magnification. Multiple-frame averaging was used to reduce noise. Color calibration of the camera (white balance) was performed using the blue-filtered, tungsten-halogen light source of the microscope, which may result in CL colors that are slightly different from other equipment (especially around the yellowish band, which is narrow), but ensures relatively standardized observation conditions.

In this study, we also present automatically reprocessed CL images (labelled as CL' in the figures) by applying the "Auto Tone" function in Photoshop. Compared with the original CL images, the CL' images typically show a better color contrast between different stages of carbonates within dolomite crystals.

3.3. SIMS $\delta^{13}C_{carb}$ analysis

In situ $\delta^{13}C_{carb}$ analysis of both calcite and dolomite was conducted on a CAMECA IMS 1280 at the Wisconsin Secondary Ion Mass Spectrometer (WiscSIMS) Laboratory, Department of Geoscience, University of Wisconsin–Madison. During SIMS analysis, carbon stable isotopes (^{12}C, ^{13}C) were measured as secondary ions when using a 7-μm-diameter primary beam. An electron flood gun in combination with a gold coating (~40 nm) was used for charge compensation. The total analytical time per spot was about 4 min including presputtering (20 s), automatic centering of the secondary ion beam in the field aperture (60 s), and analysis (160 s). The baseline noise level of the Faraday cups was monitored during presputtering. SIMS analyses were grouped in "domains" identified by SEM and CL imaging. In some cases, multiple domains were analyzed on a sample. The domains are numbered sequentially and referenced in both the appendix images and supplemental data table.

The WiscSIMS reference material UWC3 calcite was used as a running standard (Fig. A13) (Kozdon et al., 2009; Valley and Kita, 2009; Śliwiński et al., 2016). Each group of 10–15 analyses of unknown spots was bracketed by eight analyses of UWC3 to monitor running conditions. The UWC3 standard shows highly consistent $\delta^{13}C_{carb}$ values (Fig. A13; 2SD = 0.85 ‰, n = 166), demonstrating steady running conditions during WiscSIMS analytical session 2018-04-09. Carbon isotope ratios are reported in standard per mil (‰) notation relative to VPDB, calculated as $\delta^{13}C_{sample} = [(^{13}C/^{12}C)_{sample}/(^{13}C/^{12}C)_{VPDB} - 1] \times 1000$. The spot-to-spot reproducibility of $\delta^{13}C_{carb}$ values, calculated from all bracketing analyses on UWC3, is ±0.85 ‰ (averaged 2SD based on each individual bracket, 7 μm spot size, n = 166).

The raw isotope ratios obtained by SIMS are biased by an instrumental mass fractionation (IMF) that can vary in magnitude depending on instrumental conditions, mineralogy, and sample composition (Valley and Kita, 2009; Śliwiński et al., 2016). To address the effect of Fe content on the IMF of dolomite analyses, a suite of standards along the dolomite–ankerite series were analyzed at the beginning of the WiscSIMS 2018-04-09 session and used to generate a calibration curve relative to the dolomite standard UW6220 (Fig. A14).

After SIMS analysis, Fe concentration (Fe# = molar ratio of Fe/[Fe + Mg]) adjacent to each SIMS pit was measured by electron probe microanalysis (EPMA) to correct the composition-specific IMF of each SIMS $\delta^{13}C_{carb}$ analysis. Raw SIMS $\delta^{13}C_{dolomite}$ values during session 2018-04-09 were corrected based on the calibration curve in Fig. A14. Most of the analyzed dolomite spots show Fe# between 0 and 0.02 (Fig. A16), where the SIMS standards UW6220 and UWAnk10 offer a good constraint for the IMF during WiscSIMS analytical session 2018–04-09 (Fig. A14).

Raw SIMS $\delta^{13}C_{calcite}$ values during session 2018-04-09 were corrected based on the IMF of calcite standard UWC3. EPMA data show that the Huajipo calcite has average values of $MgCO_3$ = 1.07 mol%, $FeCO_3$ = 0.05 mol%, $MnCO_3$ = 1.90 mol% (n = 217), which is comparable to the UWC3 standard that has average values of $MgCO_3$ = 2.34 mol%, $FeCO_3$ = 0.76 mol%, $MnCO_3$ = 0.22 mol% (n = 51).

Cross plots of SIMS $\delta^{13}C_{carb}$ values vs. Fe and Mg concentration data show no clear correlation and an overall negative correlation between $\delta^{13}C_{carb}$ values vs. Mn concentration (Fig. A16), which is addressed in the Discussion section. All raw and corrected SIMS data, EPMA data are available in the Excel spreadsheets of the online supplementary materials.

3.4. Electron probe microanalysis

EPMA analysis was performed on the CAMECA SX-51 at the Cameron Electron Microprobe Laboratory, Department of Geoscience, University of Wisconsin-Madison. Data were collected with a ~120 s analysis time and a 15 keV, 20 nA beam, which was defocused to 5 µm diameter to minimize sample damage. Data were processed in the Probe for EPMA

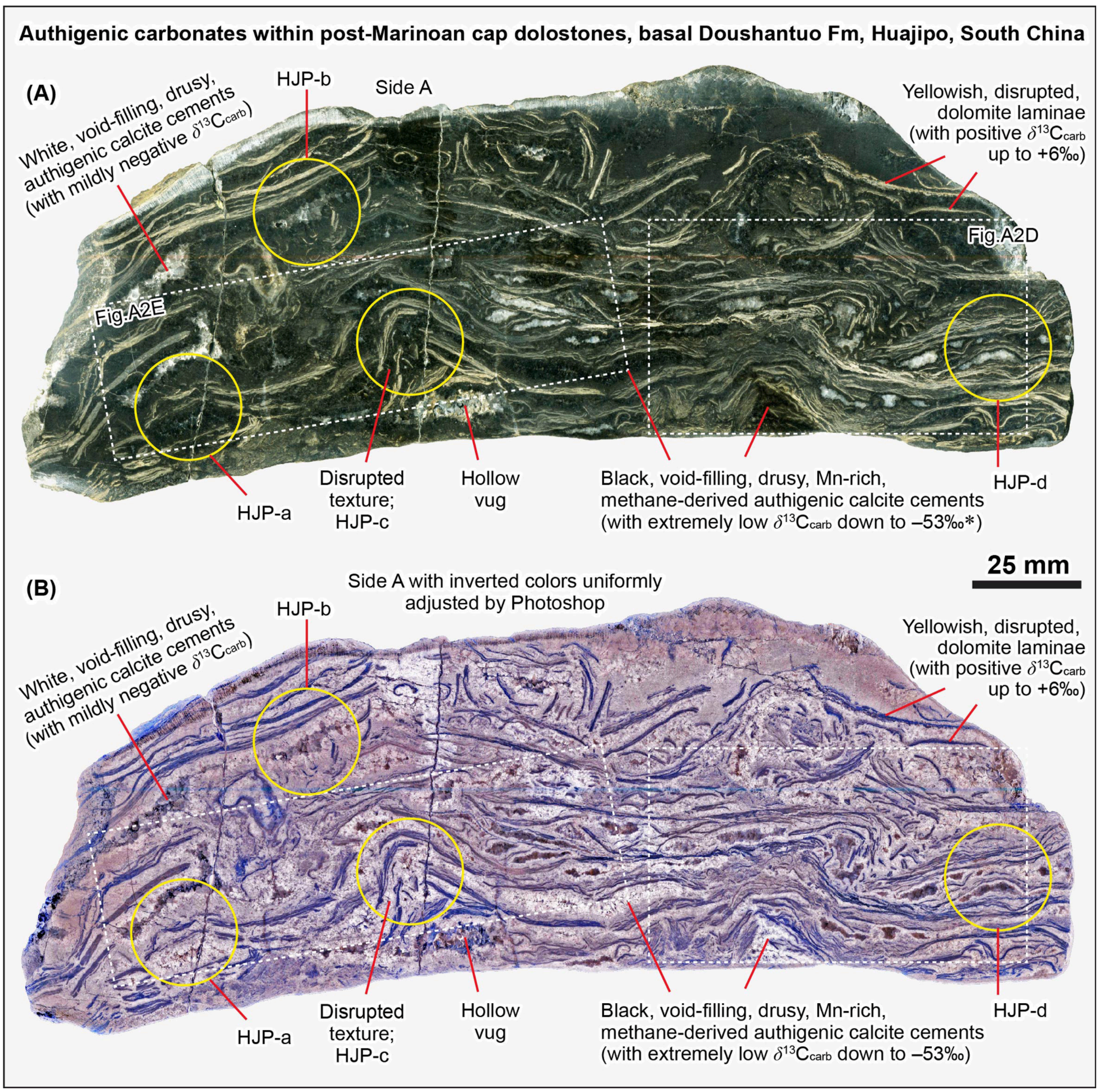

Fig. 2. Front side of the studied rock slab of authigenic carbonates within post-Marinoan cap dolostones. This sample was collected from the cap dolostone C2 interval, Doushantuo Formation, Huajipo section, South China. (A) Polished slab surface viewed with the naked eye. (B) The same view with inverted colors after applying the "Invert" function in Photoshop. Note that this slab largely shows three distinct phases: (i) Yellowish, disrupted dolomite laminae with positive $\delta^{13}C_{carb}$ signals up to +6 ‰; (ii) Black, void-filling, authigenic calcite cements with methane-derived $\delta^{13}C_{carb}$ signals down to –53 ‰; (iii) White, void-filling, blocky, authigenic calcite cements with mildly negative $\delta^{13}C_{carb}$ signals (–8‰ on average). The colors of these three authigenic phases are based on observations of polished slab with the naked eye. SEM-SIMS mounts (25.4 mm in diameter) drilled from this rock slab are shown as empty yellow circles. Dash boxes show the locations of images in Fig. A2. For comparison, previously published $\delta^{13}C_{carb}$ data based on micro-drilled powders of samples from the same stratigraphic interval could be found in the following papers (Jiang et al., 2003; Jiang et al., 2006a; Bristow et al., 2011).

software (Donovan et al., 2018), and background correction was performed using the Mean Atomic Number procedure (Donovan and Tingle, 1996). As changes over time in measured intensities are common for EPMA measurements in carbonates, particularly for the element Ca, a self-fitted time dependent intensity correction was applied for all elements (Donovan et al., 2018). CO_2 was added for the matrix correction, based upon the appropriate C:O ratio, with oxygen determined by stoichiometry to the cations. The matrix correction used was PAP, with

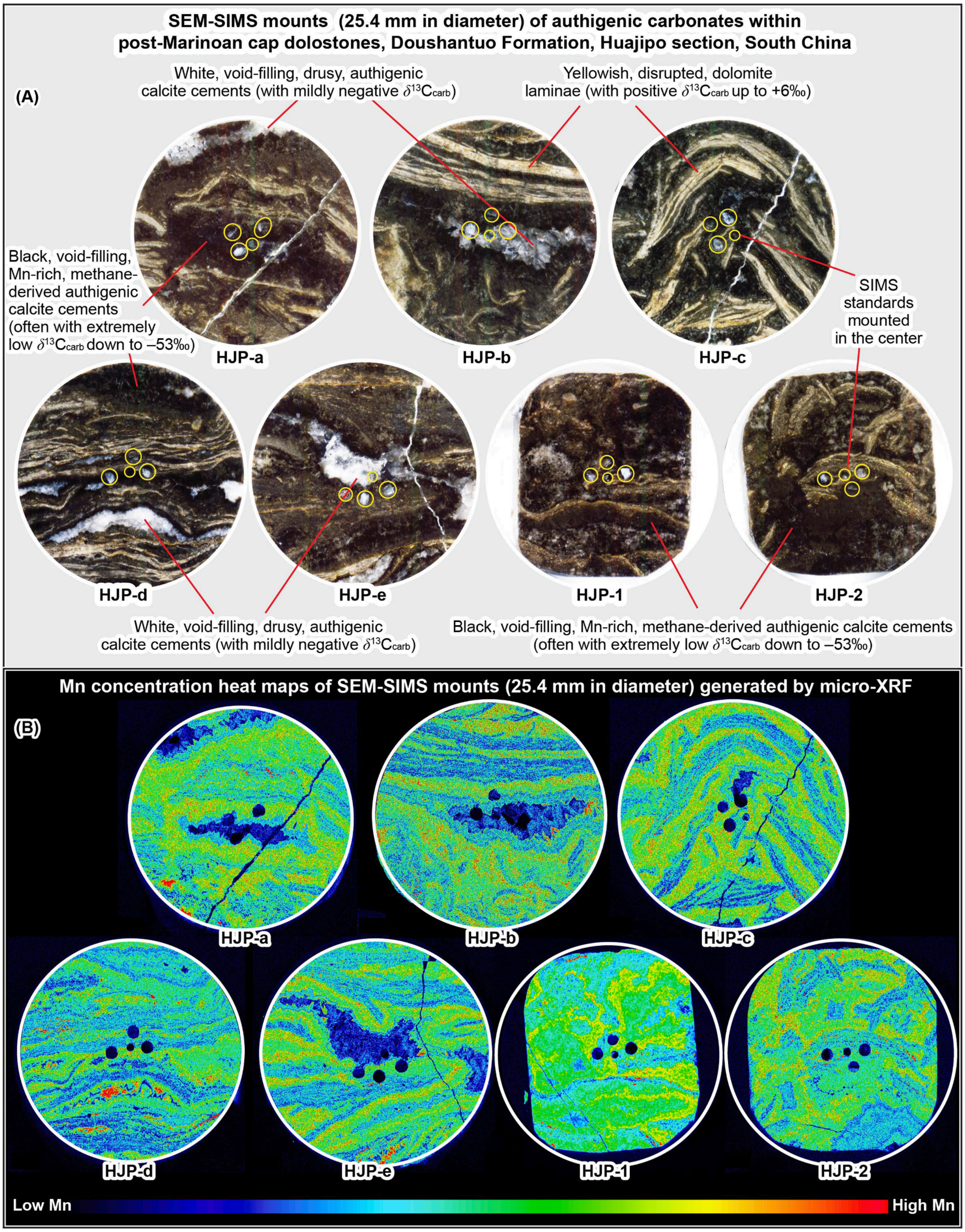

Fig. 3. SEM-SIMS mounts (25.4 mm in diameter) and corresponding elemental heat maps of authigenic carbonates within the post-Marinoan cap dolostone C2 interval, basal Doushantuo Formation, Huajipo section, South China. **(A)** SIMS mount viewed with the naked eye. SIMS standard materials were mounted in the center and marked by yellow circles in A, which were shown as black dots in B. See detailed locations of these views in Fig. 2, Fig. A1. **(B)** Mn concentration heat maps of the SEM-SIMS mounts generated by µXRF. Note that the void-filling authigenic calcite cements are overall more enriched in Mn compared with the dolomite laminae. More µXRF images are available in the online supplementary materials. Abbreviations: HJP, Huajipo; SEM, scanning electron microscope; SIMS, secondary ion mass spectrometry; µXRF, micro-X-ray fluorescence.

Henke mass absorption coefficients. Standards used were Delight Dolomite (Mg), Callender Calcite (Ca), siderite (Fe), rhodochrosite (Mn) and strontianite (Sr). Samples and standards were coated with ~200 Å carbon. WDS X-ray intensities were acquired with Probe for EPMA software, with mean atomic number backgrounds and with the PAP matrix correction and adding oxygen by stoichiometry and carbon by apportionment of C:O of 1:2, iterated within the matrix correction.

3.5. SEM imaging

After SIMS analysis, the gold coating was removed by polishing and was then replaced with an iridium coating for imaging by Scanning Electron Microscope (SEM) coupled with Energy-dispersive spectrometry (EDS) in the Ray and Mary Wilcox SEM Laboratory, Department of Geoscience, University of Wisconsin–Madison. BSE images of samples were acquired with a Hitachi S3400 VP SEM with EDS using a Thermo Fisher thin window detector. SEM images were acquired using an accelerating voltage of 15 keV at a working distance of 10 mm. All the SIMS pits were imaged by SEM and are shown with corresponding $\delta^{13}C_{carb}$ values in the online supplementary materials.

4. Integrated petrographic and geochemical results

Three authigenic carbonate phases have been identified in this study, which are yellowish disrupted dolomite laminae, black calcite cements, and white calcite cements. The colors of these above authigenic phases are based on observations of polished rock slabs with the naked eye (Fig. 2, Figs. A1, A2).

In total 289 SIMS spots have been analyzed for $\delta^{13}C_{carb}$ based on the Huajipo samples (Tables 1 and 2), including 72 SIMS spots on pure dolomite crystals, 29 SIMS spots on calcite cores of dedolomite (i.e., authigenic calcite in the form of the interiors of dedolomite crystals, see Fig. 4, Fig. A3 for typical SEM views), 145 SIMS spots on black calcite cements, and 43 SIMS spots on white calcite cements (Fig. 5, Fig. A4, Tables A1-A5). Each SIMS spot has been carefully imaged by SEM and CL and has also been analyzed by EMPA for major elements. Both the raw and the corrected SIMS $\delta^{13}C_{carb}$ data, including data measured from SIMS standard materials during the analytical session, are available in the online supplementary materials.

Table 1
A summary of the analyzed SIMS spots of authigenic carbonates within the cap dolostone C2 interval, Doushantuo Formation, Huajipo section, South China. SIMS analyses were grouped in "domains" identified by SEM and CL imaging. In some cases, multiple domains were analyzed on a sample. The domains are numbered sequentially and referenced in both the appendix images and supplemental data table. All data were analyzed during WiscSIMS session 2018–04-09 and can be found in the online supplementary materials. Abbreviations: µXRF, micro-X-ray fluorescence; N.A. = Not analyzed by SIMS; CL = cathodoluminescence; SEM = scanning electron microscope; SIMS = secondary ion mass spectrometry.

SEM-SIMS mount	µXRF	SIMS domains	SIMS pits	SEM-SIMS-CL results
HJP-a	Fig. A6	#1	@409–420	Figs. A17–18
HJP-b	Fig. A7	N.A.	N.A.	N.A.
HJP-c	Fig. A8	#1	@391–396	Fig. A19
		#2	@397–400	Fig. A20
HJP-d	Fig. A9	#1	@88–309	Figs. A21–25
		#2	@310–332	Fig. A26
		#3	@337–347	Fig. A27
		#4	@353–372	Figs. A28, 29
		#5	@373–382	Figs. A30, 31
		#6	@929–942	Figs. A29, 32
		#7	@947–977	Figs. A33–35
		#8	@978–984	Fig. A33
HJP-e	Fig. A10	#1	@584–617	Figs. A36, 37
		#2	@618–645	Fig. A38
		#3	@646–649	Fig. A39
HJP-1	Fig. A11	#1	@660–673	Fig. A40
HJP-2	Fig. A12	#1	@685–702	Fig. A41
		#2	@853–893	Fig. A42
		#3	@894–917	Fig. A43

Compared with previously published data based on conventional analysis of micro-drilled powders (~800-µm spot size) by gas-source isotope ratio mass spectrometer, our new SIMS data show the largest $\delta^{13}C_{carb}$ range (–53.1 ‰ to +6.3 ‰, VPDB) yet measured from Precambrian carbonates and a remarkably large isotopic variability at a micrometer scale (7-µm SIMS spot size). This 59.4 ‰ range was measured within a distance of 10 cm for carbonates in a single sample. Many analyzed SIMS domains show $\delta^{13}C_{carb}$ gradients of >40 ‰ within ~50 µm (See figures in Appendices). Both the negative endmember (–53.1 ‰) and the positive (up to +6.3 ‰) $\delta^{13}C_{carb}$ values are newly reported from this stratigraphic interval (Fig. 8).

4.1. Yellowish disrupted dolomite laminae

The dolomite laminae all show disrupted textures, which is consistent with observations in previous studies based on samples from the same stratigraphic interval at the same section (see Fig.13 in Jiang et al., 2006a; and Fig. 1C in Bristow et al., 2011). However, we note that these disrupted dolomite laminae consist of large (~100 to 300 µm) and euhedral dolomite crystals (Fig. 4, Fig. A3), instead of "dolomicrite" as described in previous publications (Jiang et al., 2006a; Bristow et al., 2011). In contrast with the previously published negative $\delta^{13}C_{carb}$ values from these dolomite laminae (Fig.13 in Jiang et al., 2006a; and Fig. 1C in Bristow et al., 2011), surprisingly positive $\delta^{13}C_{carb}$ values up to + 6.3 ‰ are revealed by SIMS for the first time in this study (Figs. 4-6). These positive $\delta^{13}C_{carb}$ values suggest that all the previously published negative $\delta^{13}C_{carb}$ values from these dolomite laminae likely reflect different degrees of contamination by the physical mixing with MDAC calcite (which typically has extremely negative $\delta^{13}C_{carb}$ values, see the next subsection) during sampling via micro-drill bits (~800-µm spot size). We regard that the positive $\delta^{13}C_{carb}$ data revealed by SIMS (7-µm-diameter spot size) in this study represent previously obscured and more accurate composition for these dolomite laminae.

CL results often show pink colored luminescence in dolomite cores and dull luminescence in dolomite rims (Fig. A3). Most of the dolomite cores have been replaced by calcite, showing dedolomite textures (Fig. 4, Fig. A3). Textures that show the replacement of dolomite by calcite are most obvious on the re-processed CL images (i.e., CL' images), where the residual dolomite in the core shows a pink color (see figures in Appendices for all the SIMS domains).

4.2. Black MDAC cements

Black methane-derived authigenic calcite (MDAC) cements are all void-filling and show exclusively negative $\delta^{13}C_{carb}$ values down to –53 ‰ (VPDB). Petrographic observations by SEM show that they typically occur within the space confined by disrupted dolomite laminae, with subhedral calcite along the dolomite and increasingly euhedral, bladed crystal shapes towards the center of the space (Fig. 5, Fig. A4). This petrographic relationship suggests that the black MDAC post-dates dolomite laminae.

Notably, the black MDAC cements are rich in Mn, which is consistent with a recent study (Cai et al., 2023). Cross plots of the SIMS and EPMA data show an overall negative correlation between $\delta^{13}C_{carb}$ and Mn abundance (Fig. A16). CL images of the black MDAC calcite all show bright orange luminescence (see figures of the SIMS domains in Appendices).

4.3. White calcite cements

White authigenic calcite cements are all shown as void-filling, blocky spars within the cavities of black MDAC cements. They typically have euhedral crystal boundaries and grow towards the center of the cavity.

Table 2
Sedimentological and geochemical characteristics of each individual fabric in the studied sample. The 2SD value represents two standard deviations of sample variability in each SIMS data set (not analytical precision). The value n represents the number of analyzed SIMS spots. All SEM-CL-SIMS-EPMA results are available in the online supplementary materials.

Authigenic fabrics within cap dolostones		Dolomite laminae	Calcite cores within dolomite rims	Black calcite	White calcite
Color by the naked eye		Yellowish	N.A.	Black	White
Color under CL		Dull rim, bright core	Bright	Bright	Bright
SEM petrography		Euhedral and large (>100 µm) crystals, with disrupted textures	Dolomite cores replaced by calcite	Anhedral to euhedral crystals, void-filling	Euhedral, bladed crystals, void-filling
SIMS $\delta^{13}C_{carb}$ (VPDB, ‰)	Min	0.2	–12.6	–53.1	–22.6
	Max	6.3	–1.8	–3.1	–1.9
	Mean	4.2	–4.7	–25.5	–7.9
	2SD	2.7	5.5	29.9	8.1
	n	61	29	145	43
Average elemental abundance (mol %)	Mn	0.10	1.51	2.08	1.52
	Fe	0.10	0.07	0.04	0.08
	Mg	44.37	1.70	1.02	0.82
	Ca	55.42	96.72	96.86	97.57
Interpretation		Post-depositional with respect to the cap dolostone host rock, exogeneous carbon source	Post-depositional with respect to the cap dolostone host rock, formed during dedolomitization	Post-depositional with respect to the cap dolostone host rock, post-dating the dolomite laminae	Post-depositional with respect to the cap dolostone host rock, post-dating black calcite

Some cavities remain hollow in the center, with bladed white calcite crystals as the final stage of infillings (Fig. A2).

SIMS results show that the white calcite cements all have mildly negative $\delta^{13}C_{carb}$ signals (–8‰ on average). Notably, one of the analyzed SIMS domains (i.e., SIMS domain #3 of mount HJP-e) shows white calcite (with $\delta^{13}C_{carb}$ values from –6 to –9‰) intergrowing with barite crystal fans (Fig. 4L, Fig. A39).

CL images of the white calcite all show bright orange luminescence. Elemental maps generated by µXRF show zoned features in these white calcite cements. Some white calcite cements could be strongly zoned in Mn (Fig. A9), whereas others are relatively low in [Mn] compared with the black calcite cements (Fig. A10).

5. Discussion

5.1. Paragenetic sequence

Before interpreting the geochemical data, reconstructing the paragenetic sequence for different carbonate phases strictly based on field and petrographic observations is necessary.

The cap dolostone host rock (i.e., C2 interval) at the studied Huajipo section is characterized by dolomicrite or fine-grained peloidal dolopackstone (see petrographic images Fig. 7A and B in Jiang et al., 2006a). No stromatolite or microbial mat has been found in the cap dolostone host rock. Given the contrasting features between the fine-grained cap dolostone matrix and the strongly recrystallized and disruptive dolomite laminae within the cavities, we rule out any causal link between these two dolomite phases.

Notably, samples in this study (Fig. 2, Fig. A1) were collected as authigenic carbonate infillings of cavities within the cap dolostone C2 interval. Therefore, all the three authigenic carbonate phases we analyzed by SIMS (i.e., disruptive dolomite laminae, black calcite cements, white calcite cements, see section 4 for details) are post-depositional with respect to the fine-grained cap dolostone host rock.

Petrographic results consistently show that both the black MDAC cements and the white calcite cements grow towards the center of the space confined by disrupted dolomite laminae (Fig. 5, Figs. A4, A5), suggesting that the black and white calcite cements post-date the disrupted dolomite laminae. The black calcite always grows away from the dolomite laminae, either filling the entire space or transitioning to white calcite; these relationships suggest that the black calcite cements post-dates dolomite laminae and pre-dates white calcite cements.

Petrographic observations show that white calcite is always enclosed by black calcite, and occurs in the innermost part of the cavity, suggesting a final-stage precipitation (Fig. A5). When the cavities remain open, they typically show bladed white calcite crystals growing towards the center, which further confirms that white calcite is the final stage authigenic cements in the studied sample. It is worth mentioning that in one SIMS domain (i.e., SIMS domain #3 of mount HJP-e, Fig. 4L, Fig. A39), we also observed white calcite (with $\delta^{13}C_{carb}$ values from –6 to –9‰) intergrowing with barite crystal fans, suggesting that barite cements likely precipitated at the same time with white calcite.

It is notable that dolomite crystals within the laminae commonly show euhedral and dedolomitized textures, with the dolomite interiors partially or completely replaced by calcite (Fig. 4, Fig. A3). This "inside-out" texture is common in the geological record largely due to the fact that dolomite cores are typically more unstable during diagenesis (Jones, 2005; Jones, 2007). SIMS data of the calcite cores within dedolomites show mildly negative $\delta^{13}C_{carb}$ values (–4.7 ‰ on average, n = 29). No extremely negative $\delta^{13}C_{carb}$ values that are indicative of methane oxidation (i.e., $\delta^{13}C_{carb}$ < –30 ‰, Bristow and Grotzinger, 2013) have been found in the calcite cores of dedolomites. Therefore, the diagenetic fluids that are responsible for dedolomitization are likely different from the one that caused the precipitation of black MDAC cements.

To summarize, all the three authigenic carbonate phases (i.e., yellowish dolomite laminae, black calcite cements, white calcite cements in Figs. 2, 3) are post-depositional and formed after the deposition and dissolution of host cap dolostones. Among these three carbonate phases, petrographic relationships suggest that the disrupted dolomite laminae represent the earliest precipitates. Both the black MDAC and the white calcite post-date dolomite laminae and are preserved as void-filling cements within the space confined by dolomite laminae. Black MDAC pre-dates white calcite, with the latter likely representing the final stage authigenic cements (Fig. 7).

5.2. Origin of disrupted dolomite laminae

The disrupted dolomite laminae in our samples appear enigmatic. These laminae have previously been described as "dolomicrite" (see Fig.13 in Jiang et al., 2006a; and Fig. 1C in Bristow et al., 2011) and here are revised to have been strongly disrupted, recrystallized, and dedolomitized based on detailed petrographic observations via optical microscopy, CL microscopy, and SEM (Fig. 4, Fig. A3). These laminae commonly show large (~100 to 300 µm), euhedral dolomite crystals that have been partially or completely replaced by calcite in the cores. SIMS analysis in this study show surprisingly positive $\delta^{13}C_{carb}$ signals (+0.2 to +6.3 ‰, n = 61, +4.2 ‰ on average) on dolomite spots (7-µm spot size). Considering that the post-Marinoan cap dolostones in South China (Shen et al., 2005; Jiang et al., 2010; Lang et al., 2016) and

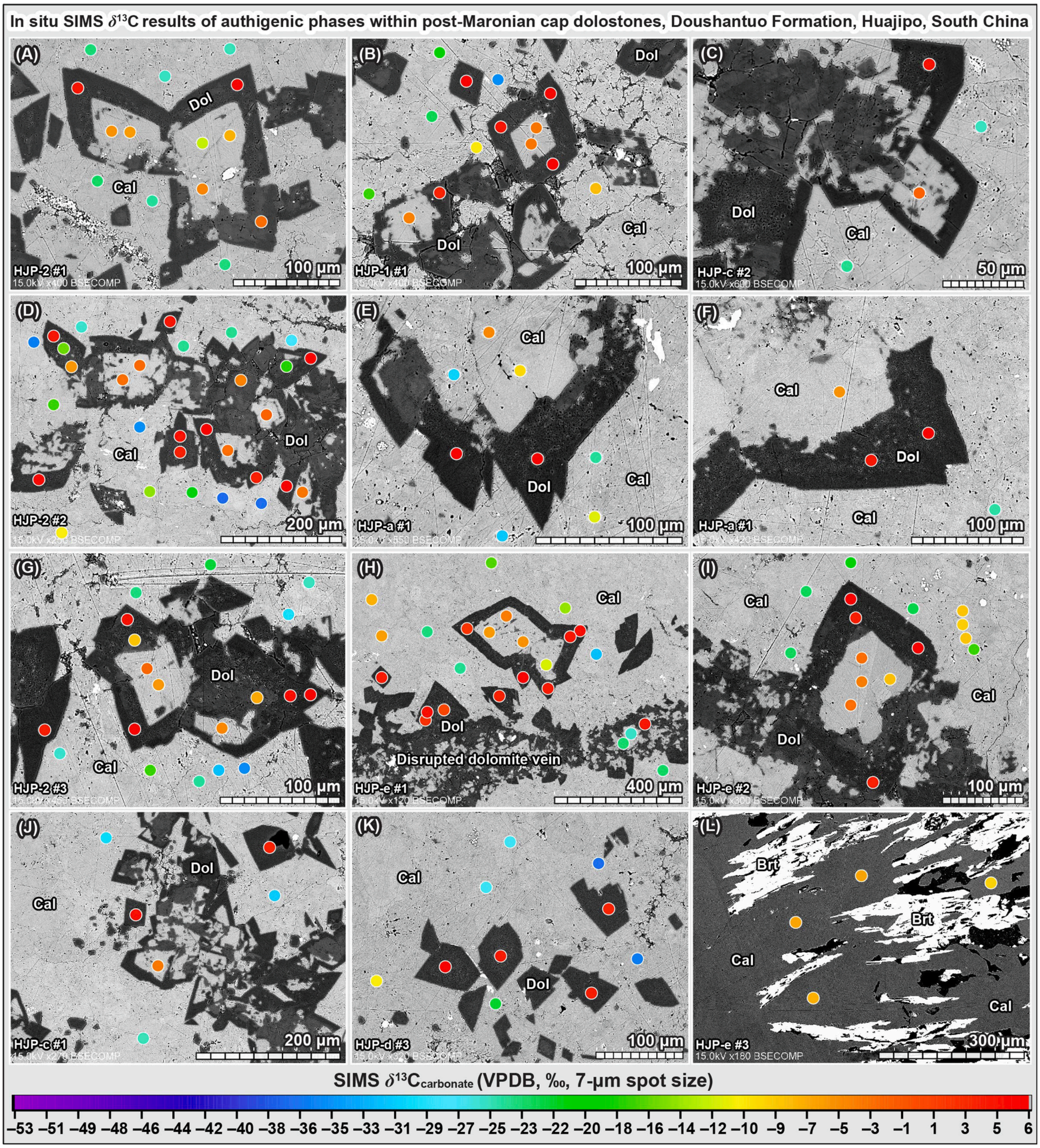

Fig.4. $\delta^{13}C_{carb}$ data (color-coded) measured in situ by SIMS on each individual authigenic carbonate phase within the post-Marinoan cap dolostone C2 interval, Doushantuo Formation, Huajipo section, South China. **(A–K)** Euhedral dolomite crystals with the interiors often replaced by calcite. The dolomite rims are typically well preserved because they are composed of diagenetically stable stoichiometric dolomite. The interiors of many dolomite crystals have been partially replaced by calcite due to its diagenetically less stable composition. The dolomite phase typically shows positive $\delta^{13}C_{carb}$ values up to +6 ‰. The calcite within dolomite core typically shows mildly negative $\delta^{13}C_{carb}$ values with a mean value of –4.7 ‰. **(L)** Barite crystal fans and white calcite cements with mildly negative $\delta^{13}C_{carb}$ values that range from –6.2 to –9.1 ‰. All the geochemical data and the corresponding petrographic context can be found in the online supplementary materials. Abbreviations: BSE, backscattered electron; Brt, barite; Cal, calcite; Dol, dolomite; HJP, Huajipo; VPDB, Vienna Pee Dee Belemnite.

beyond always show mildly negative $\delta^{13}C_{carb}$ values (mostly 0 to –5‰) (Kennedy, 1996; Hoffman et al., 1998; Hoffman et al., 2007; Rose and Maloof, 2010; Sansjofre et al., 2011; He et al., 2021; Hoffman et al., 2021), the positive $\delta^{13}C_{carb}$ values discovered in this study, therefore, are highly unusual. Two possible origins are explored below for these dolomite laminae.

5.2.1. A methanogenesis origin

It is possible that the anomalously positive $\delta^{13}C_{carb}$ signals discovered within post-Marinoan cap dolostones reflect dissolved inorganic carbon (DIC) of local porewaters. In this scenario, these positive-$\delta^{13}C_{carb}$ authigenic cements likely formed in the methanogenesis zone that was decoupled from the seawater DIC pool during an increasing burial of cap dolostones. Indeed, authigenic carbonates formed in the methanogenesis zone typically show highly positive $\delta^{13}C$ signals due to the removal of methane without oxidation. This phenomenon has been widely reported from modern marine sediments (Meister et al., 2007; Pierre et al., 2016; Phillips et al., 2018), ancient marine records (Friedman and Murata, 1979; Kokh et al., 2015; Theiling and Coleman, 2019), modern lake environments (Talbot and Kelts, 1986; Zhu et al., 2013b; Gomez et al., 2014; Birgel et al., 2015; Buongiorno et al., 2019), and ancient lake facies (Sun et al., 2020). Notably, the process of

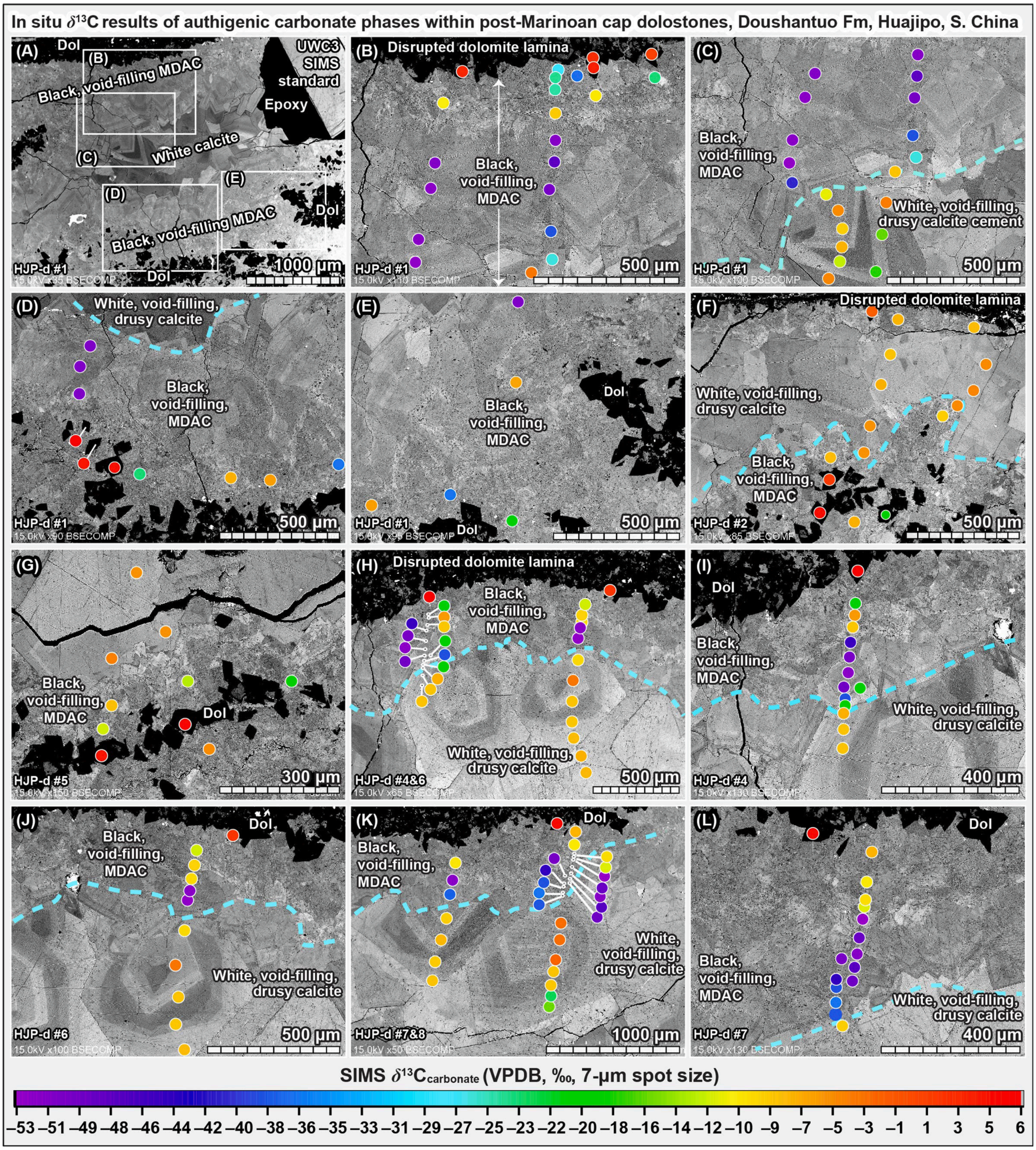

Fig. 5. SIMS $\delta^{13}C_{carb}$ data (color-coded) of authigenic carbonate phases within the cap dolostone C2 interval, Doushantuo Formation, Huajipo section, South China. Cyan dash line shows the boundary between the black MDAC and white calcite. Note that the "black" and "white" colors labelled in the figures are based on observations of polished rock slabs with the naked eye (Fig. 2, Figs. A1 and A2). This sample largely shows three distinct phases: (i) Yellowish disrupted dolomite laminae with positive $\delta^{13}C_{carb}$ signals up to +6 ‰; (ii) Black, void-filling, authigenic calcite cements with methane-derived $\delta^{13}C_{carb}$ signals down to –53 ‰; (iii) White, void-filling, blocky, authigenic calcite cements with mildly negative $\delta^{13}C_{carb}$ signals (–8‰ on average). Note that both the black MDAC and the white calcite are post-depositional, void-filling, zoned authigenic cements that grow inward within the space confined by disrupted dolomite laminae, suggesting a paragenetic sequence that post-dates the disrupted dolomite laminae. All geochemical data and the corresponding petrographic context can be found in the online supplementary materials. Abbreviations: BSE, backscattered electron; Cal, calcite; Dol, dolomite; HJP, Huajipo; MDAC, methane-derived authigenic calcite.

methanogenesis has also been proposed to occur in Precambrian water columns in order to explain many thick-bedded Precambrian strata with positive $\delta^{13}C_{carb}$ excursions (Ader et al., 2009; Cadeau et al., 2020; Cui et al., 2020).

A methanogenesis origin for these ^{13}C-enriched dolomite laminae is appealing considering that this scenario potentially fits well — in terms of isotopic mass balance — with the methane hydrate hypothesis that has been proposed based on the ^{13}C-depleted MDAC cements (Jiang et al., 2003; Jiang et al., 2006a; Wang et al., 2008; Peng et al., 2022). It is conceivable that the removal of ^{13}C-depleted methane from the methanogenesis zone may have driven porewaters (and the resulting authigenic carbonates that formed within) increasingly higher in $\delta\ ^{13}C$.

However, the scenario of marine dolomite formed within the methanogenesis zone cannot reconcile with independent field observations. Thus far, these authigenic dolomite laminae have only been found within the cavities of cap dolostone host rock. Therefore, the formation of these dolomite laminae appears to be rather local, and clearly post-depositional with respect to the cap dolostone host rock.

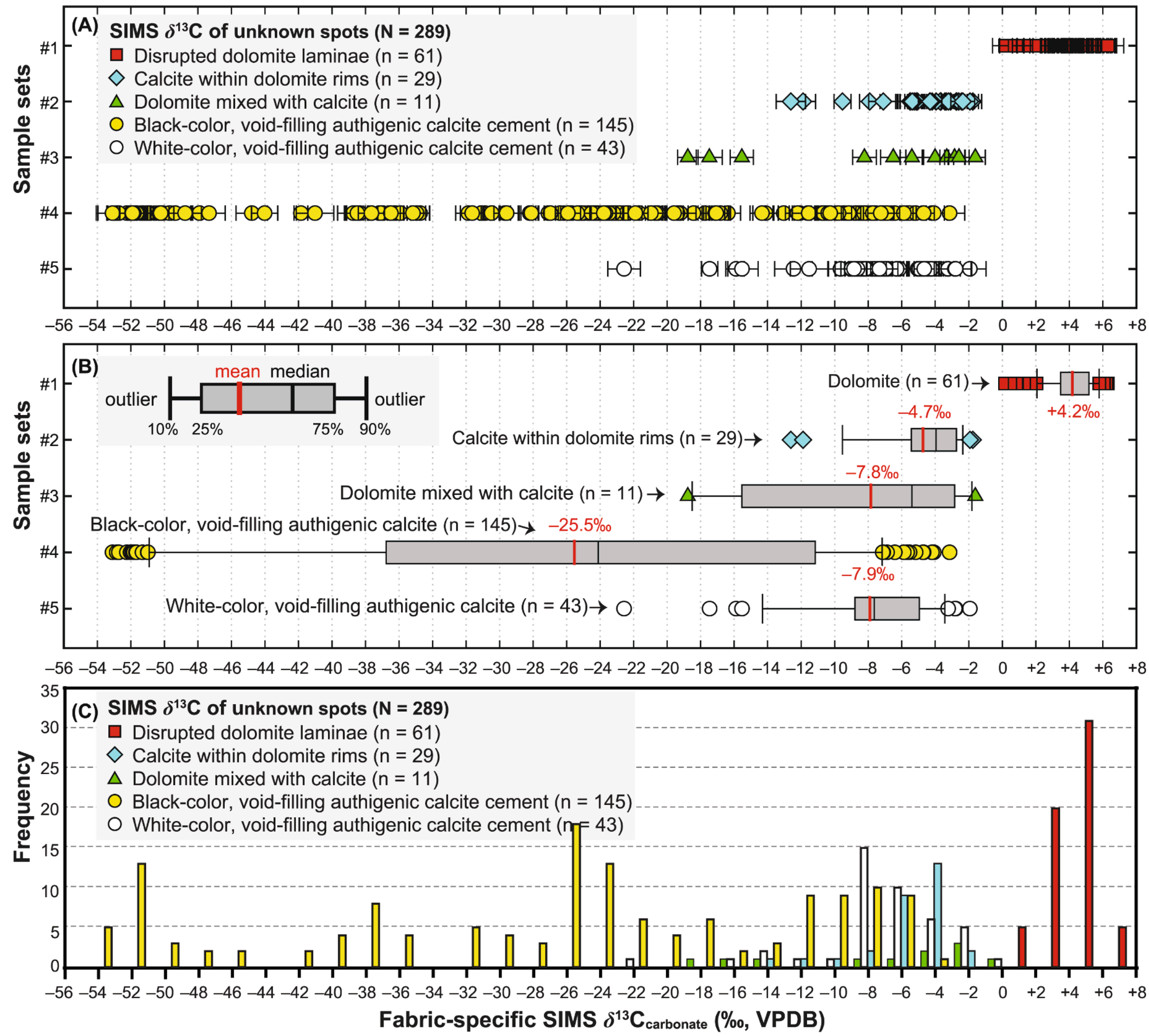

Fig. 6. Fabric-specific SIMS $\delta^{13}C_{carb}$ data analyzed in this study. All the data were analyzed from authigenic carbonates within the post-Marinoan cap dolostone C2 interval, Doushantuo Formation, Huajipo section, South China. (A) Plot of all individual SIMS analyses. (B) Box plot of the SIMS data. (C) Histogram of the SIMS data. This study, for the first time, reveals disrupted dolomite laminae with positive $\delta^{13}C_{carb}$ values up to +6 ‰ and void-filling MDAC cements with the lowest $\delta^{13}C_{carb}$ value of –53 ‰. Both the lowest (–53 ‰) and the highest (+6‰) endmember $\delta^{13}C_{carb}$ values were analyzed in situ by SIMS (7- μm spot size) and are newly reported in this study. For comparison, the $\delta^{13}C_{carb}$ data based on micro-drilled powders of samples from the same stratigraphic interval could be found in previously published papers (Jiang et al., 2003; Jiang et al., 2006a; Bristow et al., 2011). The negative $\delta^{13}C_{carb}$ values of SIMS spots that have been grouped into "Dolomite mixed with calcite" likely result from either a diagenetic process (i.e., dolomite replaced by low-$\delta^{13}C_{carb}$ calcite) or an analytical process (i.e., secondary ion bombarded both the dolomite on the surface and the underlying low-$\delta^{13}C_{carb}$ calcite in depth during SIMS analysis). All the geochemical data and the corresponding petrographic context can be found in the online supplementary materials. The distinction between black and white calcite cements is based on observations of polished rock slabs with the naked eye as shown in Fig. 2, Figs. A1, A2. Abbreviations: SIMS, secondary ion mass spectrometry; VPDB, Vienna Pee Dee Belemnite.

Second, independent petrographic observations show that the dolomite laminae in this study all consist of large (~100 to 300 μm), euhedral crystals with sharp boundaries that clearly distinguish themselves with the surrounding calcite cements (Figs. 4,5, Figs. A3, A4). Given the contrasting isotopic values between dolomite and its surrounding calcite, we preclude the possibility that these euhedral dolomite crystals formed via the recrystallization of early marine dolomicrite precursors that coexisted with MDAC. Theoretically, if the recrystallization of early marine dolomicrite indeed occurred, one would expect to see isotopic homogenization between positive-$\delta^{13}C_{carb}$ dolomicrite and its surrounding negative-$\delta^{13}C_{carb}$ MDAC; however, such a phenomenon was not seen in this study.

Based on the above considerations, we regard that a methanogenesis origin for these ^{13}C-enriched dolomite is incompatible with our field and petrographic observations and thus cannot account for the positive $\delta^{13}C_{carb}$ values measured in this study. Another explanation is required for these dolomite laminae.

5.2.2. Post-depositional dolomitizing fluids

Given the overall large size (~100 to 300 μm) and euhedral aspect of grains and the sharp crystal termination (Fig. 4), it is likely that these dolomite crystals have experienced strong recrystallization, possibly associated with late diagenetic fluids. In this study, we propose that the disrupted dolomite laminae in our samples may result from post-depositional migrations into the cap dolostones by late dolomitizing fluids that bear a distinct exogenous carbon source. In this scenario, the dolomitizing fluids may have inherited positive $\delta^{13}C_{carb}$ signals from surrounding carbonate-dominated strata (i.e., sediment-buffered diagenesis with respect to δ^{13}C) and finally led to the precipitation of authigenic dolomite laminae within the cavities of cap dolostones. Indeed, published chemostratigraphic studies of strata overlying cap dolostones show background $\delta^{13}C_{carb}$ values of ~+5‰ or slightly higher

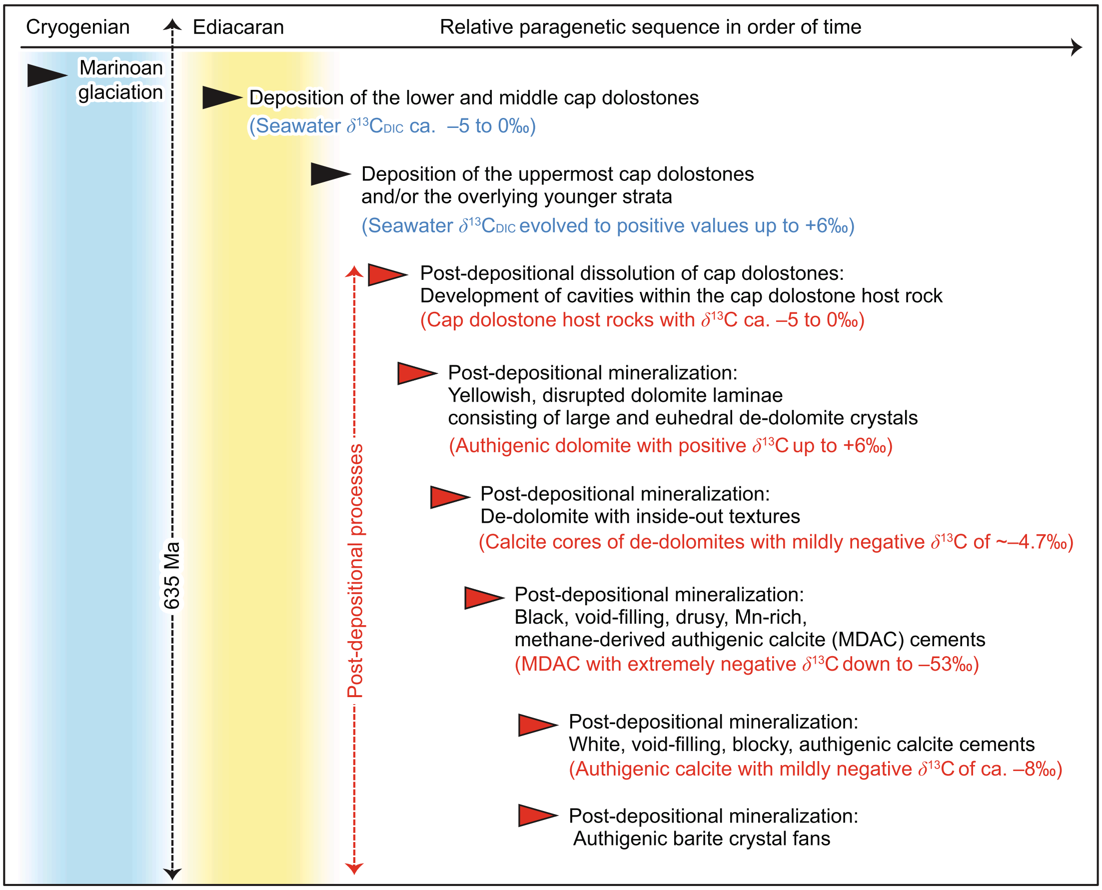

Fig. 7. Reconstructed paragenetic sequence based on integrated petrographic and in situ SIMS analysis. Note that events become younger downwards in figure. Three authigenic carbonate phases (i.e., yellowish disrupted dolomite laminae, black calcite cements, white calcite cements) have been identified based on the observations of polished rock slabs with the naked eye. All three phases are post-depositional and formed after the deposition and dissolution of host cap dolostone. Among these three carbonate phases, petrographic relationships suggest that disrupted dolomite laminae are the earliest precipitates. Both the black MDAC and the white calcite post-date dolomite laminae and are preserved as void-filling cements within the space confined by dolomite laminae. Black MDAC pre-dates white calcite and barite. In this study, we suggest that the dolomite laminae in our samples might result from migration into the cap dolostones by late dolomitizing fluids with an exogenous carbon source. See section 5.2 for detailed discussion. Abbreviations: DIC, dissolved inorganic carbon; Dol, dolomite; MDAC, methane-derived authigenic calcite.

in carbonate shelf environments (Fig. A10) (Zhou and Xiao, 2007; Zhu et al., 2007; Ader et al., 2009; Jiang et al., 2011; Johnston et al., 2012; Zhu et al., 2013a; Cui et al., 2015). In this regard, the hypothesized diagenetic fluids that bear positive $\delta^{13}C_{carb}$ signals should not be uncommon after the deposition of the uppermost cap dolostone interval.

Alternatively, the positive $\delta^{13}C_{carb}$ of post-depositional fluids could also be contemporaneous seawater when the $\delta^{13}C$ of marine DIC evolved to positive values. In this scenario, the cap dolostones might have experienced host rock dissolution and the development of cavities during a seawater regression. In a following seawater transgression, the positive $\delta^{13}C_{DIC}$ of seawater could be preserved on top of unconformities or within the cavities of the underlying cap dolostones.

5.2.3. *Age constraints for disruptive dolomite laminae*

The exact timing of this positive-$\delta^{13}C$ post-depositional dolomitizing fluid can be further constrained (Fig. 7). Based on published chemostratigraphic $\delta^{13}C_{carb}$ profiles that typically show positive $\delta^{13}C_{carb}$ values only after the deposition of the uppermost cap dolostone interval (Peng et al., 2022), the dolomitizing fluid (and the resulting dolomite laminae) should not occur until the $\delta^{13}C_{carb}$ of the marine DIC (represented as overlying bedded carbonates) evolved to positive values. In this regard, these positive-$\delta^{13}C_{carb}$ dolomite laminae should form no earlier than the deposition of the uppermost cap dolostone interval; and any positive $\delta^{13}C_{carb}$ signals found within the middle and lower cap dolostone interval likely resulted from an external dolomitizing fluid.

It is also worth mentioning that our SIMS $\delta^{13}C_{carb}$ data (7-µm spot size) are inconsistent with previously published data measured from the same dolomite laminae via micro-drilling (~800-µm spot size). SIMS data of the dolomite laminae in this study show exclusively positive values, while the previously published data (Jiang et al., 2006a; Bristow et al., 2011) show mostly negative values. We regard that the micro-drilled dolomite powders in earlier studies likely have been contaminated by the mixing of MDAC during sampling. Indeed, these dolomite laminae often show dedolomitized textures (i.e., replacement of dolomite by calcite) and are surrounded by MDAC cements with contrasting $\delta^{13}C_{carb}$ signals (Fig. 4, Fig. A3). It is, therefore, not feasible to manually sample the pure dolomite endmember via micro-drilling bits. In light of this, we regard that the previously published isotope data based on micro-drilled powders of these dolomite laminae, including the clumped isotope temperatures calculated for dolomite (Bristow et al., 2011), represent mixed signals and, therefore, are not reliable. Caution should be taken when interpreting the published data for sub-millimeter dolomite laminae.

The finding of isotopically anomalous signals in disruptive dolomite laminae within cap dolostone provides both uncertainties and opportunities. While our SIMS study offers rich new information, it is in large part based on a single sample (Fig. 2, Fig. A1). Similar dolomite laminae have not been actively searched in other cap dolostone sections in South

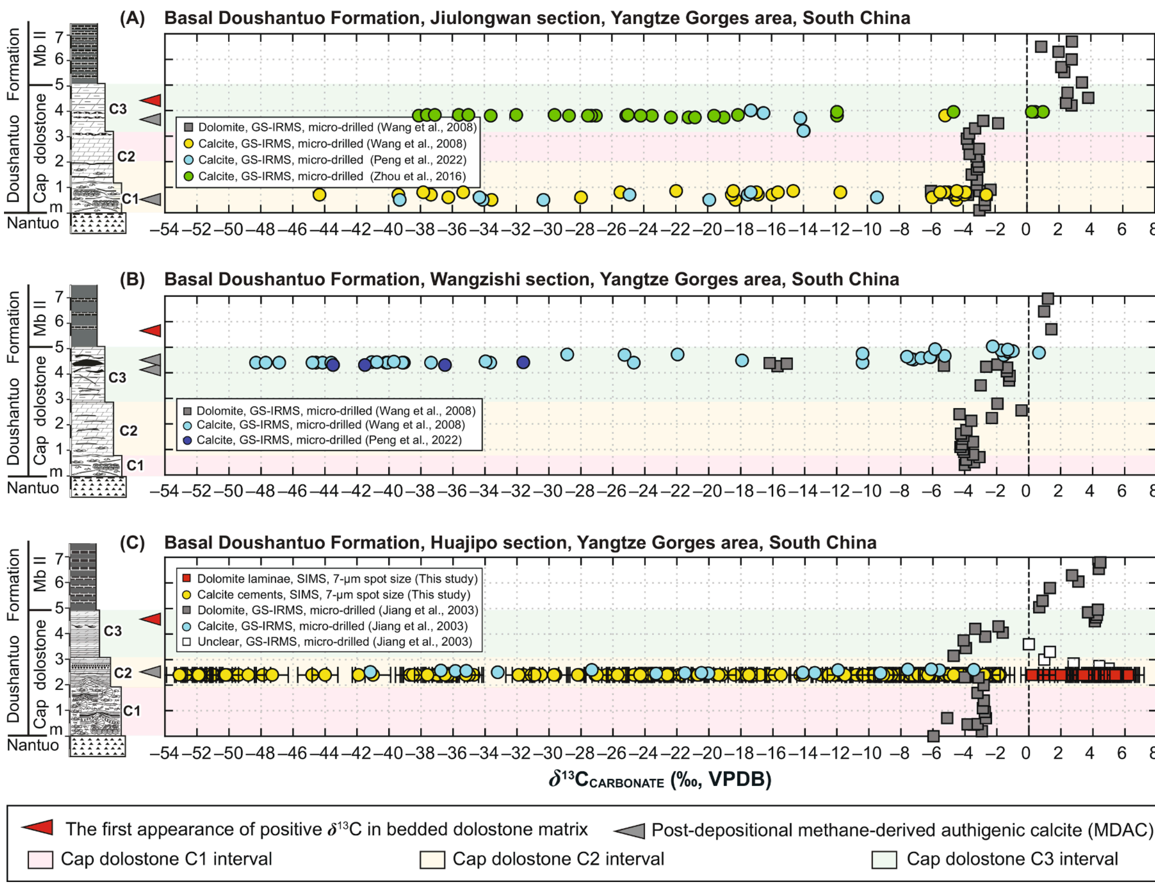

Fig. 8. Compilation of the $\delta^{13}C_{carb}$ data analyzed by GS-IRMS and SIMS. Dolomite data are shown as squares, and calcite data are shown as circles. Note that although the occurrence of MDAC is stratigraphically below the first appearance of bedded carbonate with positive $\delta^{13}C_{carb}$ values, we propose that the MDAC post-dates the uppermost cap dolostone interval and formed when seawater $\delta^{13}C_{DIC}$ had evolved to positive values. See section 5.2 for detailed discussion. Legend of the lithological columns is the same as Fig. 1. Data source: Lithological columns (Jiang et al., 2003; Jiang et al., 2006a; Wang et al., 2008), Jiulongwan dolomite data analyzed by GS-IRMS (Wang et al., 2008), Jiulongwan calcite data analyzed by GS-IRMS (Wang et al., 2008; Zhou et al., 2016; Peng et al., 2022), Wangzishi dolomite data analyzed by GS-IRMS (Wang et al., 2008), Wangzishi calcite data analyzed by GS-IRMS (Wang et al., 2008; Peng et al., 2022), Huajipo dolomite data analyzed by GS-IRMS (Jiang et al., 2003), Huajipo calcite data analyzed by GS-IRMS (Jiang et al., 2003), Huajipo SIMS data (this study). Abbreviations: GS-IRMS, gas source-isotope ratio mass spectrometry; MDAC, methane-derived authigenic calcite; SIMS, secondary ion mass spectrometry; VPDB, Vienna Pee Dee Belemnite.

China. Whether these dolomite laminae exist at a larger scale requires further investigation. It also remains to be tested whether these dolomite laminae are microbial mats or stromatolites that formed within cavities in a marine transgression after the karstification of cap dolostone. More studies are warranted to further constrain the origin, timing, and distribution of these disruptive dolomite phases in the future.

5.3. Constraints for MDAC cements

Petrographic relationships suggest that the black MDAC cements in our samples post-date the disrupted dolomite laminae that bear exotic positive $\delta^{13}C_{carb}$ signals. Given that the dolomite laminae are interpreted to have formed after the deposition of the uppermost cap dolostone interval (see section 5.2 for detailed discussion), the black MDAC cements should have formed even later.

It is notable that the MDAC cements are unusually rich in Mn compared with the dolomite laminae (Fig. 3). An overall negative correlation has been found between $\delta^{13}C_{carb}$ and Mn abundance in the MDAC cements (Fig. A16). Two scenarios could potentially explain this correlation. First, if these MDAC cements formed in a marine environment, methane oxidation by manganese oxide may have played a role during the mineralization of MDAC cements (Cai et al., 2023). Case studies about methane oxidation by manganese oxide, albeit limited, have indeed been found from the deep-time record (Hu et al., 2018; Cai et al., 2021). In this scenario, the overall negative correlation between $\delta^{13}C_{carb}$ and [Mn] likely reflects the two-endmember mixing between seawater and porewater with active methane oxidation by manganese oxide. Alternatively, these MDAC could result from a reducing, Mn(II)-rich, post-depositional diagenetic fluid. In this scenario, the overall negative correlation could reflect the different degrees of contribution by Mn(II)-rich fluids and secondary oxidation of thermogenic methane. These two scenarios remain to be further tested.

5.4. Implications for the role of methane in the wake of a snowball Earth

Our study casts doubt on the importance of methane in the wake of a snowball Earth and reveals both complexities and ambiguities. The micro-scale investigation in this study shows a remarkable new level of complex and dynamic diagenetic history with a strong post-depositional impact by exogenous fluids (Fig. 7). Importantly, our new constraints for the Huajipo MDAC (i.e., post-dating the deposition of the uppermost cap dolostones) suggest that diagenetic fluids with methane signals did not infiltrate into the Doushantuo cap dolostones until the $\delta^{13}C$ of seawater DIC had already evolved to positive values. In contrast with previous studies (Kennedy et al., 2001; Jiang et al., 2003; Jiang et al., 2006a; Kennedy et al., 2008), our interpretation for MDAC does not support the views that gas hydrate destabilization and oxidation accounts for the overall negative $\delta^{13}C$ excursion (~−5‰) in cap dolostones or have played any critical role right after the Marinoan glaciation. In addition, the late infiltration of methane-bearing fluids within cap dolostones also casts doubt on the practice of using MDAC as a marker bed for stratigraphic correlation (Peng et al., 2022).

When precisely the authigenic carbonates in this study formed remains unclear. Due to the remarkable micro-scale heterogeneity – both petrographically and isotopically – of these carbonates, direct geochronological dating is challenging. Previously published U-Pb dating for these carbonates by laser ablation all yield rather large errors (Lan et al., 2022; Shi et al., 2023) and are, therefore, ambiguous when interpreting its paragenetic relationship with different stages of authigenic phases. That said, our independent constraint for the timing of the Huajipo MDAC is consistent with an earlier study by Zhou et al. (2010), which also suggests that methane signals postdate the deposition and a later karstification of cap dolostones based on field and petrographic observations.

6. Conclusions

This study focuses on the controversial authigenic carbonate cements within the post-Marinoan cap dolostone C2 interval, Doushantuo Formation at Huajipo, South China (Fig. 1). These isotopically anomalous cements have been arguably – and equally controversially – interpreted as the ^{13}C-depleted methane seep remnants in the geological record. Detailed SEM-SIMS-CL-µXRF analyses have been conducted on these enigmatic cements in this study.

Our new SIMS data (7-µm SIMS spot size) show the largest $\delta^{13}C_{carb}$ range (–53.1 ‰ to +6.3 ‰, VPDB) yet measured from Precambrian carbonates and remarkable isotopic variability at a micrometer scale. Many analyzed SIMS domains show $\delta^{13}C_{carb}$ gradients of >40 ‰ within ~50 µm (See Appendices figures). Both the most negative (–53.1 ‰) and the most positive (+6.3 ‰) $\delta^{13}C_{carb}$ values are newly reported from this stratigraphic interval.

Integrated petrographic and geochemical results show three distinct phases of authigenic carbonates, which are all post-depositional, preserved collectively as infillings of a carbonate cavity within the cap dolostone host rock. The relative timing of these three authigenic phases is listed below in the order of paragenetic sequence. (i) Yellowish (colors observed by the naked eye, the same hereafter) disrupted dolomite laminae with positive $\delta^{13}C_{carb}$ signals up to + 6.3 ‰. (ii) Black, void-filling, methane-derived authigenic calcite (MDAC) cements with extremely negative $\delta^{13}C_{carb}$ signals as low as –53.1 ‰; (iii) White, void-filling, blocky, authigenic calcite cements with mildly negative $\delta^{13}C_{carb}$ signals (–8‰ on average).

The dolomite laminae all show disrupted, recrystallized, and dedolomitized textures that suggest a strong influence by post-depositional fluids. Surprisingly positive $\delta^{13}C_{dolomite}$ values up to + 6.3 ‰ are revealed by SIMS for the first time within post-Marinoan cap dolostones. We suggest that the dolomite laminae with an obvious exogeneous carbon signal formed after the deposition of the uppermost cap dolostone interval, and the black MDAC formed even later. Both the positive and the extremely negative $\delta^{13}C_{carb}$ represent post-depositional exogenous carbon sources that are irrelevant to the snowball Earth deglaciation.

The black MDAC cements in our samples are unusually rich in Mn. An overall negative correlation between $\delta^{13}C_{carb}$ and Mn abundance indicates the involvement of methane oxidation by manganese oxide. It also remains possible that MDAC resulted from a reducing, Mn(II)-rich diagenetic fluid with secondary oxidation of thermogenic methane.

The new constraint for MDAC in this study (i.e., post-dating the deposition of the uppermost cap dolostones) challenges the hypothesis that gas hydrate destabilization and oxidation accounts for the overall negative δ^{13}C excursion (~–5‰) in cap dolostones and/or have played a critical role in Snowball Earth deglaciation. The late infiltration of methane-bearing fluids within cap dolostones also casts doubt on the practice of using MDAC as a marker bed for stratigraphic correlation.

Contributions

HC designed research; HC and MJS prepared SIMS samples; HC and IJO performed SIMS analysis assisted by KK and JWV at the WiscSIMS laboratory; HC and JHF performed SEM and EPMA analyses; KK, IJO, AD, and HC corrected raw SIMS data; HC and JMB performed CL analysis; HC, NJW, and SG conducted µXRF analysis; HC interpreted the results and wrote the manuscript with contributions from all coauthors. All authors contributed to discussion and manuscript revision.

Data availability

Integrated SIMS, SEM, µXRF, CL, and EDS results of authigenic carbonates within Marinoan cap dolostones from the Doushantuo Formation at Huajipo, South China (PowerPoint slides) are available through figshare at https://dx.doi.org/10.6084/m9.figshare.23994207. Spreadsheets of SIMS carbon isotope data and EPMA elemental concentration data of all analyzed spots on authigenic carbonates within post-Marinoan cap dolostones from the Doushantuo Formation at Huajipo, South China (Excel spreadsheets) are available through figshare at https://dx.doi.org/10.6084/m9.figshare.23994213.

Declaration of competing interest

The authors declare that they have no known competing financial interests or personal relationships that could have appeared to influence the work reported in this paper.

Acknowledgements

The authors want to sincerely thank Ganqing Jiang (UNLV) for sharing the samples that were previously studied by Jiang et al., (2006a) and offering constructive and open-minded comments on this study. We also thank Brian Hess, Noriko Kita, James Kern, Maciej Śliwiński, and Akizumi Ishida for assistance in sample preparation and SIMS analysis at UW-Madison; Bil Schneider (UW-Madison), Stephan Borensztajn and Bénédicte Ménez (IPGP) for assistance in the SEM laboratories; Yiheng Wu for assistance in compiling the supplemental materials. Although the views are those of the authors, many small questions or confusions have been clarified via kind discussions with the following colleagues over the years. They are Chuanming Zhou (NIGPAS), Yongbo Peng (NJU), Huiming Bao (NJU), Shuhai Xiao (VT), Taiyi Luo (IGCAS), Tian Gan (UMD), Xianguo Lang (CDUT), Jing Huang (IOCAS), Fei Li (SWPU), Zhou Wang (CUG-Wuhan), Zhongwu Lan (IGGCAS), Magali Bonifacie (IPGP), and Chaojin Lu (Miami).

This study was supported by the NASA Astrobiology Institute (NNA13AA94A) at UW-Madison. The WiscSIMS Lab was supported by NSF (EAR-1658823, -2004618) and UW-Madison. JWV was also supported by NSF (EAR-1524336) and DOE (DE-FG02-93ER14389). The XRF lab was supported by VUB strategic research funding. This paper benefits from constructive and detailed reviews by Paul F. Hoffman (Harvard & Victoria), Eva E. Stüeken (St Andrews), and two other anonymous reviewers. The authors thank Associate Editor Eva E. Stüeken and Executive Editor Jeffrey G. Catalano (WUSTL) for their efficient handling of this manuscript. Huan Cui dedicates this paper to his former academic advisor Dr. Ping Guan (Professor Emeritus of Sedimentary Geology), who recently retired from the Department of Geology at Peking University, for the lively and respectful mentorship and the practical hands-on research experience that HC received from 2008 to 2011 in different oil fields in China.

Appendix A. Supplementary material

The Appendix includes integrated geochemical and petrographic results of individual SIMS domains. **Figs. A1–A2**, polished rock slabs of authigenic carbonates within post-Marinoan cap dolostones from the

Doushantuo Formation at Huajipo, South China; **Figs. A3–A5**, petrographic results showing paragenetic relationship among the three distinct authigenic carbonate phases; **Figs. A6–A12**, SEM-SIMS mounts (25.4 mm in diameter) and corresponding SEM and µXRF images; **Fig. A13**, time-series SIMS carbon isotope data analyzed in this study during WiscSIMS analytical session 2018-04-09; **Fig. A14**, SIMS carbon isotope bias during WiscSIMS analytical session 2018-04-09 plotted against Fe# [= molar ratio of Fe/(Mg+Fe)]; **Fig. A15**, corrected SIMS carbon isotope data of each individual mount. **Fig. A16**, Cross-plots of SIMS data vs. elemental abundances; **Figs. A17–A43**, integrated SEM and SIMS results of each analyzed domains of authigenic carbonates within post-Marinoan cap dolostones from the Doushantuo Formation at Huajipo, South China; **Tables A1–A5**, SIMS carbon isotope data that are grouped into each individual petrographic texture. Supplementary material to this article can be found online at https://doi.org/10.1016/j.gca.2023.11.002.

References

Ader, M., et al., 2009. A multilayered water column in the Ediacaran Yangtze platform? Insights from carbonate and organic matter paired $\delta^{13}C$. Earth Planet. Sci. Lett. 288, 213–227.

Ahm, A.-S.-C., et al., 2019. An early diagenetic deglacial origin for basal Ediacaran "cap dolostones". Earth Planet. Sci. Lett. 506, 292–307.

Álvaro, J.J., Billström, K., Hallmann, C., Hoshino, Y., Jorge, A., 2023. Ediacaran cap carbonates with microbial build-ups capping barite-bearing methane seep networks in the Kaarta Mountains, Taoudeni Basin. Mali. Sedimentary Geol. 455, 106481.

Bao, H., et al., 2000. Anomalous ^{17}O compositions in massive sulphate deposits on the Earth. Nature 406, 176–178.

Birgel, D., et al., 2015. Methanogenesis produces strong ^{13}C enrichment in stromatolites of Lagoa Salgada, Brazil: a modern analogue for Palaeo-/Neoproterozoic stromatolites? Geobiology 13, 245–266.

Bristow, T.F., Bonifacie, M., Derkowski, A., Eiler, J.M., Grotzinger, J.P., 2011. A hydrothermal origin for isotopically anomalous cap dolostone cements from south China. Nature 474, 68–71.

Bristow, T.F., Grotzinger, J.P., 2013. Sulfate availability and the geological record of cold-seep deposits. Geology 41, 811–814.

Buongiorno, J., Gomez, F.J., Fike, D.A., Kah, L.C., 2019. Mineralized microbialites as archives of environmental evolution, Laguna Negra, Catamarca Province, Argentina. Geobiology 17, 199–222.

Cadeau, P., et al., 2020. Carbon isotope evidence for large methane emissions to the Proterozoic atmosphere. Sci. Rep. 10, 18186.

Cai, C., et al., 2021. Anaerobic oxidation of methane by Mn oxides in sulfate-poor environments. Geology 49, 761–766.

Cai, C., et al., 2023. Interlinked marine cycles of methane, manganese, and sulfate in the post-Marinoan Doushantuo cap dolostone. Geochim. Cosmochim. Acta 346, 245–258.

Campbell, K.A., 2006. Hydrocarbon seep and hydrothermal vent paleoenvironments and paleontology: Past developments and future research directions. Palaeogeogr. Palaeoclimatol. Palaeoecol. 232, 362–407.

Cao, X., Bao, H., 2013. Dynamic model constraints on oxygen-17 depletion in atmospheric O_2 after a snowball Earth. Proc. Natl. Acad. Sci. 110, 14546–14550.

Condon, D., et al., 2005. U-Pb ages from the Neoproterozoic Doushantuo Formation, China. Science 308, 95–98.

Crockford, P.W., et al., 2016. Triple oxygen and multiple sulfur isotope constraints on the evolution of the post-Marinoan sulfur cycle. Earth Planet. Sci. Lett. 435, 74–83.

Crockford, P.W., et al., 2018. Linking paleocontinents through triple oxygen isotope anomalies. Geology 46, 179–182.

Cui, H., et al., 2015. Redox architecture of an Ediacaran ocean margin: Integrated chemostratigraphic ($\delta^{13}C$–$\delta^{34}S$–$^{87}Sr/^{86}Sr$–Ce/Ce*) correlation of the Doushantuo Formation, South China. Chem. Geol. 405, 48–62.

Cui, Y., et al., 2019. Germanium/silica ratio and rare earth element composition of silica-filling in sheet cracks of the Doushantuo cap carbonates, South China: constraining hydrothermal activity during the Marinoan snowball Earth glaciation. Precambr. Res. 105407.

Cui, H., et al., 2020. Global or regional? Constraining the origins of the middle Bambuí carbon cycle anomaly in Brazil. Precambr. Res. 348, 105861.

Cui, H., et al., 2021. Deposition or diagenesis? Probing the Ediacaran Shuram excursion in South China by SIMS. Global Planet. Change 206, 103591.

Cui, H., et al., 2022. An authigenic response to Ediacaran surface oxidation: remarkable micron-scale isotopic heterogeneity revealed by SIMS. Precambr. Res. 377, 106676.

de Winter, N.J., Claeys, P., 2017. Micro X-ray fluorescence (µXRF) line scanning on Cretaceous rudist bivalves: a new method for reproducible trace element profiles in bivalve calcite. Sedimentology 64, 231–251.

de Winter, N.J., Sinnesael, M., Makarona, C., Vansteenberge, S., Claeys, P., 2017. Trace element analyses of carbonates using portable and micro-X-ray fluorescence: performance and optimization of measurement parameters and strategies. J. Anal. At. Spectrom 32, 1211–1223.

Donovan, J.J., Tingle, T.N., 1996. An improved mean atomic number background correction for quantitative microanalysis. Microsc. Microanal. 2, 1–7.

Donovan, J.J., Kremser, D., Fournelle, J., Goemann, K., 2018. Probe for Windows User's Guide and Reference, Enterprise Edition. Probe Software Inc, Eugene, OR.

Fabre, S., Berger, G., 2012. How tillite weathering during the snowball Earth aftermath induced cap carbonate deposition. Geology 40, 1027–1030.

Fabre, S., Berger, G., Chavagnac, V., Besson, P., 2013. Origin of cap carbonates: an experimental approach. Palaeogeogr. Palaeoclimatol. Palaeoecol. 392, 524–533.

Friedman, I., Murata, K., 1979. Origin of dolomite in Miocene Monterey Shale and related formations in the Temblor Range, California. Geochim. Cosmochim. Acta 43, 1357–1365.

Gan, T., et al., 2021. Cryptic terrestrial fungus-like fossils of the early Ediacaran Period. Nat. Commun. 12, 641.

Gomez, F.J., Kah, L.C., Bartley, J.K., Astini, R.A., 2014. Microbialites in a high-altitude Andean lake: multiple controls in carbonate precipitation and lamina accretion. PALAIOS 29, 233–249.

He, R., Lang, X., Shen, B., 2021. A rapid rise of seawater $\delta^{13}C$ during the deglaciation of the Marinoan Snowball Earth. Global Planet. Change 103672.

Hoffman, P.F., et al., 2007. Are basal Ediacaran (635 Ma) post-glacial "cap dolostones" diachronous? Earth Planet. Sci. Lett. 258, 114–131.

Hoffman, P.F., 2011. Strange bedfellows: glacial diamictite and cap carbonate from the Marinoan (635 Ma) glaciation in Namibia. Sedimentology 58, 57–119.

Hoffman, P.F., et al., 2017. Snowball Earth climate dynamics and Cryogenian geology–geobiology. Sci. Adv. 3, e1600983.

Hoffman, P.F., et al., 2021. Snowballs in Africa: sectioning a long-lived Neoproterozoic carbonate platform and its bathyal foreslope (NW Namibia). Earth Sci. Rev. 219, 103616.

Hoffman, P.F., Macdonald, F.A., 2010. Sheet-crack cements and early regression in Marinoan (635 Ma) cap dolostones: Regional benchmarks of vanishing ice-sheets? Earth Planet. Sci. Lett. 300, 374–384.

Hoffman, P.F., Macdonald, F.A., Halverson, G.P., 2011. Chapter 5. Chemical sediments associated with Neoproterozoic glaciation: iron formation, cap carbonate, barite and phosphorite. In: Arnaud, E., Halverson, G.P., Shields-Zhou, G. (Eds.), The Geological Record of Neoproterozoic Glaciations. Geological Society, London, Memoirs, London, pp. 67–80.

Hoffman, P.F., Schrag, D.P., 2002. The snowball Earth hypothesis: testing the limits of global change. Terra Nova 14, 129–155.

Hoffman, P.F., Kaufman, A.J., Halverson, G.P., Schrag, D.P., 1998. A Neoproterozoic Snowball Earth. Science 281, 1342–1346.

Hoffmann, K.-H., Condon, D.J., Bowring, S.A., Crowley, J.L., 2004. U-Pb zircon date from the Neoproterozoic Ghaub Formation, Namibia: Constraints on Marinoan glaciation. Geology 32, 817–820.

Hu, W.-X., et al., 2018. Thermochemical oxidation of methane induced by high-valence metal oxides in a sedimentary basin. Nat. Commun. 9, 5131.

Huang, K.-J., et al., 2016. Episode of intense chemical weathering during the termination of the 635 Ma Marinoan glaciation. Proc. Natl. Acad. Sci. 113, 14904–14909.

Jiang, G., et al., 2010. Organic carbon isotope constraints on the dissolved organic carbon (DOC) reservoir at the Cryogenian-Ediacaran transition. Earth Planet. Sci. Lett. 299, 159–168.

Jiang, G., Kennedy, M.J., Christie-Blick, N., 2003. Stable isotopic evidence for methane seeps in Neoproterozoic postglacial cap carbonates. Nature 426, 822–826.

Jiang, G., Kennedy, M.J., Christie-Blick, N., Wu, H., Zhang, S., 2006a. Stratigraphy, sedimentary structures, and textures of the late Neoproterozoic Doushantuo cap carbonate in South China. J. Sediment. Res. 76, 978–995.

Jiang, G., Shi, X., Zhang, S., 2006b. Methane seeps, methane hydrate destabilization, and the late Neoproterozoic postglacial cap carbonates. Chin. Sci. Bull. 51, 1152–1173.

Jiang, G., Shi, X., Zhang, S., Wang, Y., Xiao, S., 2011. Stratigraphy and paleogeography of the Ediacaran Doushantuo Formation (ca. 635–551Ma) in South China. Gondw. Res. 19, 831–849.

Johnston, D.T., Macdonald, F.A., Gill, B.C., Hoffman, P.F., Schrag, D.P., 2012. Uncovering the Neoproterozoic carbon cycle. Nature 483, 320–323.

Jones, B., 2005. Dolomite crystal architecture: Genetic implications for the origin of the Tertiary dolostones of the Cayman Islands. J. Sediment. Res. 75, 177–189.

Jones, B., 2007. Inside-out dolomite. J. Sediment. Res. 77, 539–551.

Kennedy, M.J., 1996. Stratigraphy, sedimentology, and isotopic geochemistry of Australian Neoproterozoic postglacial cap dolostones; deglaciation, $\delta^{13}C$ excursions, and carbonate precipitation. J. Sediment. Res. 66, 1050–1064.

Kennedy, M.J., Christie-Blick, N., Sohl, L.E., 2001. Are Proterozoic cap carbonates and isotopic excursions a record of gas hydrate destabilization following Earth's coldest intervals? Geology 29, 443–446.

Kennedy, M., Mrofka, D., von der Borch, C., 2008. Snowball Earth termination by destabilization of equatorial permafrost methane clathrate. Nature 453, 642–645.

Killingsworth, B.A., Hayles, J.A., Zhou, C., Bao, H., 2013. Sedimentary constraints on the duration of the Marinoan Oxygen-17 Depletion (MOSD) event. Proc. Natl. Acad. Sci. 110, 17686–17690.

Kokh, S.N., et al., 2015. Heavy carbon travertine related to methane generation: a case study of the Big Tarkhan cold spring, Kerch Peninsula, Crimea. Sed. Geol. 325, 26–40.

Kozdon, R., Ushikubo, T., Kita, N.T., Spicuzza, M., Valley, J.W., 2009. Intratest oxygen isotope variability in the planktonic foraminifer *N. pachyderma*: Real vs. apparent vital effects by ion microprobe. Chem. Geol. 258, 327–337.

Lan, Z., et al., 2022. Geochronological and geochemical constraints on the origin of highly $^{13}C_{carb}$-depleted calcite in basal Ediacaran cap carbonate. Geol. Mag. 159, 1323–1334.

Lang, X., et al., 2016. Ocean oxidation during the deposition of basal Ediacaran Doushantuo cap carbonates in the Yangtze Platform, South China. Precambr. Res. 281, 253–268.

Lin, Z., Wang, Q., Feng, D., Liu, Q., Chen, D., 2011. Post-depositional origin of highly ^{13}C-depleted carbonate in the Doushantuo cap dolostone in South China: insights from petrography and stable carbon isotopes. Sed. Geol. 242, 71–79.
Liu, C., Wang, Z., Macdonald, F.A., 2018. Sr and Mg isotope geochemistry of the basal Ediacaran cap limestone sequence of Mongolia: Implications for carbonate diagenesis, mixing of glacial meltwaters, and seawater chemistry in the aftermath of Snowball Earth. Chem. Geol. 491, 1–13.
Meister, P., et al., 2007. Dolomite formation in the dynamic deep biosphere: results from the Peru Margin. Sedimentology 54, 1007–1032.
Ning, M., Yang, F., Ma, H., Lang, X., Shen, B., 2021. Precipitation of Marinoan cap carbonate from Mn-enriched seawater. Earth Sci. Rev. 218, 103666.
Peckmann, J., Thiel, V., 2004. Carbon cycling at ancient methane–seeps. Chem. Geol. 205, 443–467.
Peng, Y., et al., 2022. A transient peak in marine sulfate after the 635-Ma snowball Earth. Proc. Natl. Acad. Sci. 119.
Peng, Y., Bao, H., Zhou, C., Yuan, X., 2011. ^{17}O-depleted barite from two Marinoan cap dolostone sections, South China. Earth Planet. Sci. Lett. 305, 21–31.
Phillips, S.C., Hong, W.-L., Johnson, J.E., Fahnestock, M.F., Bryce, J.G., 2018. Authigenic carbonate formation influenced by freshwater inputs and methanogenesis in coal-bearing strata offshore Shimokita, Japan (IODP site C0020). Mar. Pet. Geol. 96, 288–303.
Pierre, C., et al., 2016. Mineralogical, geochemical and isotopic characterization of authigenic carbonates from the methane-bearing sediments of the Bering Sea continental margin (IODP Expedition 323, Sites U1343–U1345). Deep Sea Res. Part II 125–126, 133–144.
Prave, A.R., Condon, D.J., Hoffmann, K.H., Tapster, S., Fallick, A.E., 2016. Duration and nature of the end-Cryogenian (Marinoan) glaciation. Geology 44, 631–634.
Rose, C.V., Maloof, A.C., 2010. Testing models for post-glacial 'cap dolostone' deposition: Nuccaleena Formation, South Australia. Earth Planet. Sci. Lett. 296, 165–180.
Sansjofre, P., et al., 2011. A carbon isotope challenge to the snowball Earth. Nature 478, 93–96.
Shen, Y., Zhang, T., Chu, X., 2005. C-isotopic stratification in a Neoproterozoic postglacial ocean. Precambr. Res. 137, 243–251.
Shi, H., et al., 2023. U-Pb age of highly ^{13}C-depleted calcite from the basal Ediacaran cap carbonate in Yichang, Hubei Province. J. Stratigr. 47, 1–16 (in Chinese with an English abstract).
Shields, G.A., 2005. Neoproterozoic cap carbonates: a critical appraisal of existing models and the plumeworld hypothesis. Terra Nova 17, 299–310.
Shields, G.A., Deynoux, M., Strauss, H., Paquet, H., Nahon, D., 2007. Barite-bearing cap dolostones of the Taoudéni Basin, northwest Africa: sedimentary and isotopic evidence for methane seepage after a Neoproterozoic glaciation. Precambr. Res. 153, 209–235.
Śliwiński, M.G., et al., 2016. Secondary ion mass spectrometry bias on isotope ratios in dolomite–ankerite, Part II: δ^{13}C matrix effects. Geostand. Geoanal. Res. 40, 173–184.
Sun, F., et al., 2020. Methanogen microfossils and methanogenesis in Permian lake deposits. Geology 49, 13–18.
Talbot, M.R., Kelts, K., 1986. Primary and diagenetic carbonates in the anoxic sediments of Lake Bosumtwi, Ghana. Geology 14, 912–916.
Theiling, B.P., Coleman, M., 2019. The relationship of diagenesis with a complex microbial ecosystem in the phosphatic interval of the Miocene Monterey Formation: evidence from stable isotopes and mineralogy. Mar. Geol. 413, 112–128.
Valley, J.W., Kita, N.T., 2009. *In situ* oxygen isotope geochemistry by ion microprobe. In: Fayek, M. (Ed.), Secondary Ion Mass Spectrometry in the Earth Sciences – Gleaning the Big Picture from a Small Spot. Mineralogical Association of Canada Short Course 41, Toronto, pp. 19–63.
Wang, Z., et al., 2017. Raman geothermometry of carbonaceous material in the basal Ediacaran Doushantuo cap dolostone: the thermal history of extremely negative δ13C signatures in the aftermath of the terminal Cryogenian snowball Earth glaciation. Precambr. Res. 298, 174–186.
Wang, J., Jiang, G., Xiao, S., Li, Q., Wei, Q., 2008. Carbon isotope evidence for widespread methane seeps in the ca. 635 Ma Doushantuo cap carbonate in south China. Geology 36, 347–350.
Wang, Y., Lu, S., Gao, Z., Lin, W., Ma, G., 1981. Sinian Tillites of China. In: Hambrey, M. J., Harland, W.B. (Eds.), Earth's Pre-Pleistocene Glacial Record. Cambridge University Press, Cambridge, Great Britain, pp. 386–401.
Wei, G.-Y., et al., 2019. Ca and Sr isotope constraints on the formation of the Marinoan cap dolostones. Earth Planet. Sci. Lett. 511, 202–212.
Xiao, S., et al., 2012. Integrated chemostratigraphy of the Doushantuo Formation at the northern Xiaofenghe section (Yangtze Gorges, South China) and its implication for Ediacaran stratigraphic correlation and ocean redox models. Precambr. Res. 192–195, 125–141.
Xiao, S., et al., 2020. Using SIMS to decode noisy stratigraphic δ^{13}C variations in Ediacaran carbonates. Precambr. Res. 343, 105686.
Yang, C., et al., 2021. The tempo of Ediacaran evolution. Science. Advances 7, eabi9643.
Yang, J., Jansen, M.F., Macdonald, F.A., Abbot, D.S., 2017. Persistence of a freshwater surface ocean after a snowball Earth. Geology 45, 615–618.
Zhang, S., et al., 2005. U-Pb sensitive high-resolution ion microprobe ages from the Doushantuo Formation in south China: constraints on late Neoproterozoic glaciations. Geology 33, 473–476.
Zhou, C., Bao, H., Peng, Y., Yuan, X., 2010. Timing the deposition of ^{17}O-depleted barite at the aftermath of Nantuo glacial meltdown in South China. Geology 38, 903–906.
Zhou, C., Guan, C., Cui, H., Ouyang, Q., Wang, W., 2016. Methane-derived authigenic carbonate from the lower Doushantuo Formation of South China: Implications for seawater sulfate concentration and global carbon cycle in the early Ediacaran ocean. Palaeogeogr. Palaeoclimatol. Palaeoecol. 461, 145–155.
Zhou, G., Luo, T., Zhou, M., Xing, L., Gan, T., 2017. A ubiquitous hydrothermal episode recorded in the sheet-crack cements of a Marinoan cap dolostone of South China: implication for the origin of the extremely ^{13}C-depleted calcite cement. J. Asian Earth Sci. 134, 63–71.
Zhou, C., Xiao, S., 2007. Ediacaran δ^{13}C chemostratigraphy of South China. Chem. Geol. 237, 89–108.
Zhu, M., et al., 2013a. Carbon isotope chemostratigraphy and sedimentary facies evolution of the Ediacaran Doushantuo Formation in western Hubei, South China. Precambr. Res. 225, 7–28.
Zhu, Z., Chen, J.A., Zeng, Y., 2013b. Abnormal positive δ13C values of carbonate in Lake Caohai, southwest China, and their possible relation to lower temperature. Quat. Int. 286, 85–93.
Zhu, M., Zhang, J., Yang, A., 2007. Integrated Ediacaran (Sinian) chronostratigraphy of South China. Palaeogeogr. Palaeoclimatol. Palaeoecol. 254, 7–61.